SATURATED FLOW BOILING IN SMALL- TO MICRO- DIAMETER METALLIC TUBES: EXPERIMENTAL RESULTS AND MODELING

T.G. Karayiannis, D. Shiferaw and D.B.R. Kenning

Brunel University, School of Engineering and Design, West London, Uxbridge, Middlesex, UB8 3PH, UK
tassos.karayiannis@brunel.ac.uk

ABSTRACT

Some results of a long-term study of flow boiling patterns, heat transfer rates and pressure drop of R134a at pressures of 6-14 bar in five vertical stainless steel tubes of internal diameter 4.26, 2.88, 2.01, 1.1 and 0.52 mm are presented in this paper. The flow regimes in the 4.26 mm to 1.1 mm tubes were identified as dispersed bubble, bubbly, slug, churn, annular and mist flows. As the diameter was reduced, progressively slimmer vapour slugs, a thinner liquid film around the vapour slug and a less chaotic vapour-liquid interface in churn flow were observed. Confined flow appeared first in the 2.01 mm tube. Dispersed bubble flow was not observed in the smallest tube (0.52 mm) for the range studied in runs in which wavy film flow occurred. The heat transfer coefficients in tubes ranging from 4.26 mm down to 1.1 mm increased with heat flux and system pressure, but did not change with vapour quality for low quality values. At higher quality, the heat transfer coefficients decreased with quality, indicating local dryout. The heat transfer characteristics of the 0.52 mm tube were different from those in the larger tubes. The data fell into two groups that exhibited different influences of heat flux below and above a heat flux threshold. The pressure drop and heat transfer results were compared with existing correlations but with some limited success. Recent progress on mechanistic models for heat transfer along with comparisons and recommendations are included in the paper.

1. INTRODUCTION

Flow boiling in large channels

Current developments in microelectronics and power electronics depend on the removal of heat at high heat fluxes. The miniaturization and intensification of power and refrigeration systems and chemical processes also require the transfer of high heat fluxes at low temperature differences (high heat transfer coefficients $\alpha = q/\Delta T$) to achieve efficient use of energy. Saturated flow boiling is an effective means of transferring heat across a thin liquid film to a liquid - vapour interface that is approximately at the saturation temperature corresponding to the local pressure, so that $\Delta T = T_w - T_{sat}$, the wall superheat. A practical advantage is that the bulk temperature of the coolant decreases slightly axially, whereas the temperature of a single-phase coolant increases. The vapour then transports the heat to a remote location but the liquid evaporated from the film must be replenished: if the wall dries out for an extended period, the heat transfer coefficient is greatly reduced. This may occur if the local heat flux is too high (critical heat flux), or if the heated flow channel is so long that the thermodynamic quality x (mass fraction of vapour) approaches unity at the exit (dryout). Heat transfer and dryout may be influenced by oscillations in the flow due to the combination of the compressibility of vapour with the inertia of liquid and interaction of the conditions in one heated channel with other parallel channels and the rest of the flow system. Reliable (but not highly accurate) methods have been developed for the design of systems employing flow boiling in large channels, for the moment crudely defined as having cross-sectional dimensions exceeding say 5 - 10 mm. The methods generally depend on correlations of large experimental data banks, guided by simplified models for physical processes dependent on the geometrical arrangement of the liquid and vapour (the flow pattern or regime). A widely used approach is to assume that heat is transferred by a combination of nucleate boiling and convective boiling. In nucleate boiling, thin liquid films are created cyclically under small bubbles growing in contact with the wall at individual nucleation sites, the number of which depend on the microgeometry (roughness) of the wall and the wall superheat. The heat transfer coefficient increases nonlinearly with increasing heat flux but is insensitive to the flow rate through the channel. In convective boiling, heat is transferred from the wall through the laminar sublayer to the turbulent flow of the mixture of liquid and bubbles that have detached from the wall and coalesced. The heat transfer coefficient depends on the resulting flow pattern but is nearly independent of the heat flux. The flow pattern depends on the flow rate and the local quality and is not very sensitive to upstream conditions. This is fortunate, because most laboratory experiments are performed with axially uniform heat flux, unlike many industrial applications. Typical data for water flowing up a vertical 9.6 mm internal diameter tube plotted as α vs. x are shown in figure 1, [1]. A correlation for the convective contribution to heat transfer α_c , valid at low wall superheat and/or high quality, obtained for a large number of data shown in figure 2(a), is included in this figure. F is the ratio of α_c to α_l , the heat transfer coefficient for the same total mass flow as liquid. The flow patterns in large channels are influenced by their orientation in the gravitational field. Application of the same correlation to data for a 14.4 mm tube leads to deviations as parallel lines at $J_g^* < 1$, where J_g^* is a non-dimensional superficial vapour velocity dependent on the ratio of inertia to buoyancy stresses, figure 2(b) :

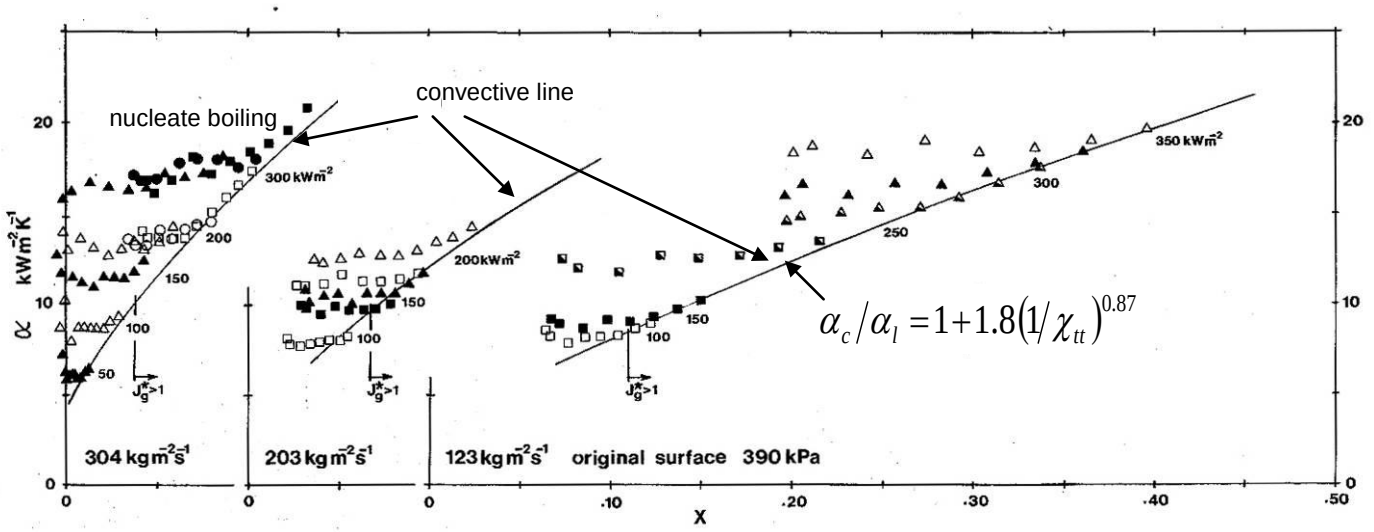

Fig.1."Apparently nucleate" and convective boiling, water in 9.6 mm tube, Kenning and Cooper [1].

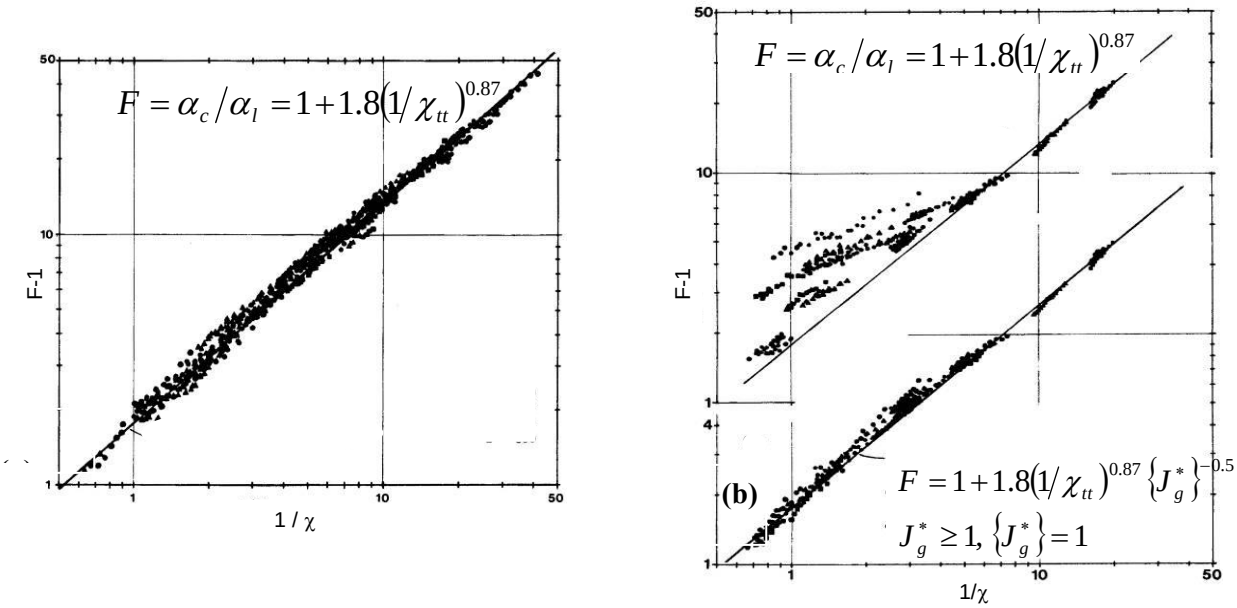

Fig.2. Correlation for convective boiling, water at 170-590 kPa (a) 9.6 mm tube, (b) 14.4 mm tube, [1].

$$J_g^* = \left[\rho_g U_g^2 / gD(\rho_g - \rho_g)\right]^{0.5} = Gx/\left[gD\rho_g(\rho_l - \rho_g)\right]^{0.5} \qquad (1)$$

The predictions of heat transfer coefficient have to be accompanied by predictions of the pressure gradient in the channel to calculate the pumping power and also the gradient of T_{sat} , the local reference temperature for heat transfer.

Flow boiling in small channels

It is difficult to couple thermally a small, intense source of heat and a boiling channel of large cross-section. The thermal resistance external to the channel may be reduced by replacing one large channel by many smaller channels in parallel, figure 3(a). Also, the heat transfer area is used more effectively, so that a nominal heat flux of 3 MW/m^2 at the source may correspond to ~ 1 MW/m^2 at the boiling surface. For a wall superheat of say 30 K, the required heat transfer coefficient is 33 kW/m^2 K, equivalent to steady conduction through a liquid film of thickness 20 μm in water or 3 μm in refrigerant R134a. Heat transfer coefficients of this order are approached for water in a 9.6 mm diameter tube in figure 1 and, as shown later in the paper, for R134a in a 0.52 mm tube (but at a lower heat flux). The practical problem is to maintain the film so that dry patches do not develop, either through evaporation to dryness or instabilities driven by hydrodynamic and capillary stresses. Reduction in the channel cross-section dimension D leads to thinner liquid films, which may improve heat transfer, and laminar instead of turbulent flow in the upstream regions of low quality, which may have the opposite effect. Stresses due to surface tension σ scale as σ/D and transverse gradients of capillary pressure drive liquid towards the corners of a non-circular cross-section, figure 3(b). Surface tension exerts greater influence on the motion of bubbles. Individual bubbles may grow rapidly to fill the channel cross-section, forming a train of confined bubbles (slug flow) that coalesce at higher quality to form annular flow. The reduction in surface area reduces the number of nucleation sites available to produce bubbles per unit length of the channel and bubble growth may induce large fluctuations in pressure that interact with bubble nucleation and cause flow reversal.

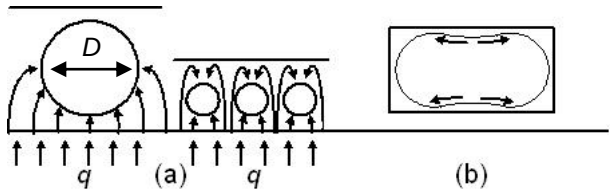

Figure 3. Effect of channel size and shape.

Boiling heat transfer depends on the thermal and surface properties of the heated wall, as well as the liquid-vapour flow and the channel cross-section. Rectangular or triangular cooling channels may be micromachined directly into silicon wafers, or machined into metal heat sinks for thermal bonding to silicon chips. Metal heat exchangers may be fabricated by diffusion bonding of electromachined plates, assembled from drawn circular tubing or aluminium extrusions with multiple internal passages. Metals differ from silicon in their thermal and wetting properties and in the nature of their surface roughness.

With this variety of applications and the changes in the physics of flow boiling as the channel size is reduced, it is unsurprising that there has been mixed success with attempts to adapt the methods of correlating boiling heat transfer coefficients in large tubes, of the sort illustrated in figures 1, 2, to smaller channels. Comprehensive reviews of the data and comparisons with correlations are available, e.g. in [2,3]. There is disagreement about the threshold size below which channels may be regarded as small, (with further divisions into mini- or micro-), instead of large. Criteria may be specified simply as ranges of diameter (hydraulic diameter if non-circular) or by physical arguments based on the relative scale of the stresses due to surface tension (σ /D), buoyancy ($\Delta\rho gD$), inertia (ρU^2) and viscosity ($\mu U/D$). With several ratios to choose from, it is unclear whether changes from "large" to "small" behaviour may occur at a narrow or broad threshold, at a single threshold or several. For large tubes, figure 2(b) and Eq. (1), it appears that the ratio of inertia and buoyancy determines a rather sharp flow regime transition that influences heat transfer. A physics-based criterion for the first threshold between large and small tubes has been based on the ratio of surface tension and buoyancy stresses expressed as Confinement number *Co* [4], Eotvos number *Eo* [5] or Bond number Bo [6] :

$$Co > 0.5, \quad Co = [\sigma/\Delta\rho\, g]^{1/2}/D \qquad (2)$$

$$Eo < 1.6, \quad Eo = \Delta\rho\, gD^2/\sigma \qquad (3)$$

$$Bo < 0.3, \quad Bo = 1/Co \qquad (4)$$

There is wide disagreement between the predicted threshold diameters, in the ratio 1, 0.63, 0.15. Kew and Cornwell deduced their criterion [4] by equating the buoyancy-driven detachment diameter of a bubble to the tube diameter. The Eotvos number is also used to specify the maximum diameter for the formation of long confined vapour bubbles during the initial filling of pulsating heat pipes, as reviewed by Zhang and Faghri [7]. Other ratios that exclude gravity are used to characterize steady adiabatic flows in small tubes: Reynolds number $Re = \rho UD/\mu$, Weber number $We = \rho U^2 D/\sigma$, density ratio, ρ_l/ρ_v . In theoretical studies, the gas density is often assumed to be negligible, so that $\rho = \rho_l$. The Capillary number $Ca = Re/We = \sigma/\mu U$, the ratio of viscous to surface tension stresses, defines non-dimensional features of adiabatic confined-bubble flow in small tubes at low Reynolds number, such as the ratio of the liquid film thickness round the bubbles to the diameter *D*,[8]. The influence of inertia depends on *Re* but a more convenient parameter may be the non-dimensional diameter $F = Ca\ Re = D\rho\sigma/\mu^2$, because it contains only *D* and fluid properties [9].

These non-dimensional parameters define steady flows but they do not take into account inertial stresses due to the axial acceleration inherent in flow boiling, which becomes very large as the channel cross section *D* is reduced at fixed mass flux *G* and heat flux *q,* as will be discussed later in this paper. Acceleration may modify the shapes of bubbles and the thickness of liquid films [10]. If the incoming liquid flow is laminar in very small channels, liquid slugs trapped between expanding confined vapour bubbles may be accelerated through the conventional *Re* criterion for laminar-turbulent transition, which may not apply at high accelerations. The relatively low accelerations for flow boiling in large channels, in which the incoming flow is usually turbulent, are consistent with the heat transfer correlations and flow regime maps based on local conditions and the fruitful analogy between flow patterns in boiling and in simpler experiments in adiabatic gas-liquid flows. It is unclear whether this approach will always be valid for boiling in small channels.

The experimental data for boiling heat transfer in small channels are not extensive so tests of correlations tend to use all the data that are available for single and parallel channels of all cross-sectional shapes. Thome [3] remarked on the poor agreement between data from different laboratories for the same fluid at the same nominal conditions. This may be due to the difficulty of making measurements on very small channels, or it may indicate that significant rig-dependent secondary effects have been ignored. These include:

- Bubble nucleation dependent on inlet subcooling and Reynolds number and on the availability of nucleation sites. On metal surfaces with randomly distributed sites, the small surface area of micro-channels may lead to significant statistical variations between individual channels. Smooth silicon surfaces may cause difficulties in initiating nucleation that may be offset in a controlled manner by providing micro-machined sites [11-14]. In some experiments, subcooled liquid containing an unknown concentration of dissolved gas that would aid nucleation is fed to a boiling channel, either following circulation through a tank open to the atmosphere, or by using gas pressure to drive the liquid flow.
- Pressure fluctuations due to the acceleration of liquid slugs by the formation and growth of individual confined bubbles. The fluctuations may cause flow reversal if there is some compressibility in the incoming flow [15-18], or if fluid can be diverted to parallel channels through an inlet plenum. It has been shown that the reversal can be suppressed by a localized

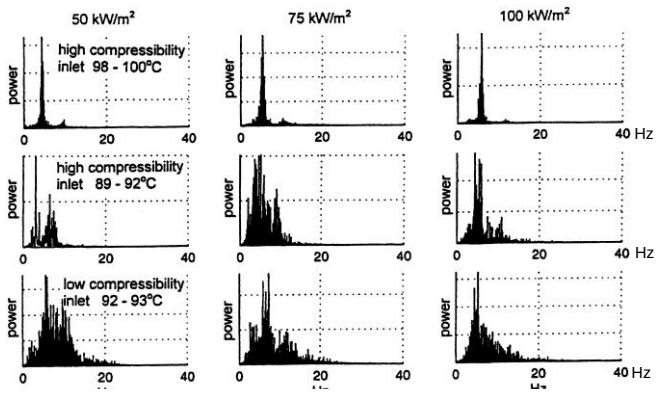

Figure 4. Pressure fluctuation power densities, effect of inlet conditions and heat fluxes, water at 101 kPa, 134 kg/m^{2}s in 2 x 1mm channel [15].

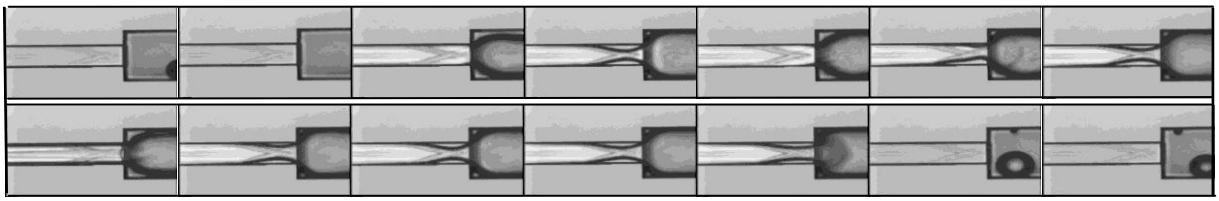

Figure 5. Exit flow, water at 101 kPa in 100 μm channel, Lian Zhang (private communication).

restriction in each channel at the inlet, e.g. [19], or a more distributed restriction due to a gradual change in channel cross-section, [20]. The absence of flow reversal does not remove the pressure fluctuations but may change their power spectrum, figure 4. The fluctuations are influenced by the channel exit conditions, [15]. The influence of channel exit geometry has received little attention in micro-channel studies. An example of transient flow disturbances at the exit from a rectangular silicon channel of mean hydraulic diameter 100 μm is shown in figure 5, recorded by Dr Lian Zhang (private communication) during research at Stanford University described in [11, 12].

The high-frequency pressure fluctuations cause local fluctuations in saturation temperature and the consequent variations in wall superheat may be of similar magnitude to the mean superheat driving heat transfer, modifying the processes of bubble nucleation and growth that drive the fluctuations [14]. It will be shown later in this paper that the fluctuations should be smaller in high pressure systems.

- Vapour inception before the heated channel.

First nucleation inside the channel may not necessarily occur if it is supplied with a mixture of liquid and vapour

(i) from a refrigeration cycle,

(ii) by accumulation of vapour in the inlet plenum feeding parallel channels due to flow reversals or axial conduction,

(iii) by flashing due to the pressure drop across restrictions at the inlets to individual channels, installed to prevent flow reversal.

Investigation of flow boiling of R134a in metal tubes

As discussed above, the understanding of two-phase flow in small and micro channels is still very limited and calls for more research work, see also recent reviews by Celata [21] and earlier by Thome [3]. A long-term experimental study of flow boiling patterns, heat transfer rates and pressure drop of R134a in five vertical stainless steel tubes of internal diameter 4.26, 2.88, 2.01, 1.1 and 0.52 mm was undertaken to provide a consistent set of data for the effect of reduction in diameter for a wide range of flow rates and pressures. The tube diameters were chosen to span the threshold for large to small tube behaviour as predicted by Confinement or Eotvos number criteria, but not the much smaller diameters based on Bond number, Table 1. The experimental methods and results are described in Section 2. Flow visualization results are included in Section 3. Pressure drop and heat transfer results as well as comparisons with correlations are presented in Sections 4 and 5 respectively. The mechanisms of heat transfer are discussed in Section 6, which includes comparisons with the mechanistic 3-zone model of Thome et al. [22, 23] and some developments in 1-D models.

Table 1. Threshold for departure from macro-size behaviour

	Air/water	R134a		
Pressure (bar)	1.0	6.0	10.0	14
Temperature (^oC)	25.0	21.6	31.3	52.5
Criterion	Critical diameter (mm)			
C=0.5	5.5	1.71	1.61	1.36
Eö=1.6	3.5	1.08	1.02	0.86
Bo=0.3	0.83	0.26	0.24	0.20

2. EXPERIMENTAL FACILITY AND PROCEDURE

The experimental facility at Brunel University was described elsewhere and only a brief description will be given here for completeness, see Huo et al. [24] and Chen et al. [25]. The test facility, which is shown in figure 6, consists of three main systems, i.e. the R134a main circuit, data acquisition and control, and the R22 cooling system. It was designed to allow testing of single and multichannel systems, different fluids and a wide range of flow conditions. The five test sections were made of stainless steel cold drawn tubes, see figure 7. They were heated by the direct passage of alternating electric current. Fifteen K-type thermocouples that were spot-welded to the outside of the tube at a uniform spacing were used to record the outer wall temperatures for the 4.26 mm to 1.1 mm tubes. The first and last thermocouple readings were not used in the analysis so as to avoid errors due to thermal conduction to the electrodes. Ten thermocouples were spot-welded on the 0.52 mm tube – the two at each end were located sufficiently far from the electrodes to be used in the data analysis. The pressures and temperatures at the inlet and outlet were measured using pressure transducers and T-type thermocouples. A differential pressure transducer was installed across the test section to provide the pressure drop measurement. The flow patterns were recorded at the exit of the heating section through a borosilicate glass tube, see figure 7. A digital high-speed camera (Phantom V4 B/W, 512 x 512 pixels resolution, 1000 pictures/sec with full resolution and maximum 32000 pictures/sec with reduced resolution, 10 ms exposure time) was used to observe the flow patterns.

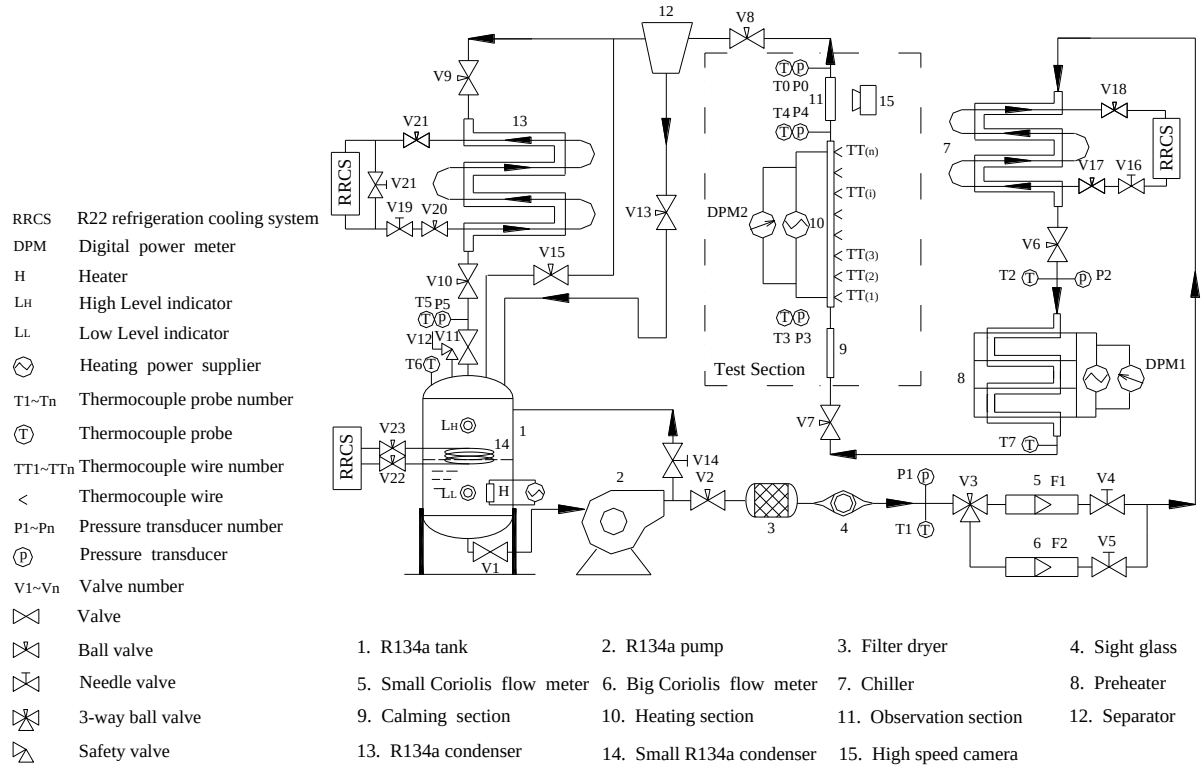

Figure 6. Schematic diagram of the system, [24].

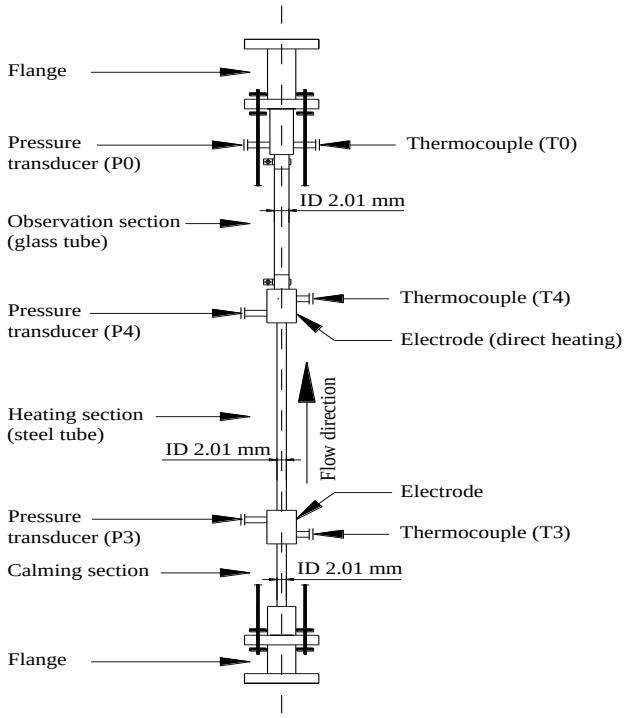

Figure 7. Schematic of the test section assembly, [25].

The inlet conditions for all the experiments were single-phase liquid at low subcooling (1-5 K) achieved by adjusting the capacity of the chiller and heating power to the preheater. The flow rate was set to the required value and the heat flux was increased in small steps until the exit quality reached about 90 %. The data were recorded after the system was steady at each heat flux, which normally took about 15 minutes but sometimes longer. Each recording was the average of 20 measurements.

Heat Transfer Coefficient

Equation 5 below was used to calculate the local heat transfer coefficient $\alpha(z)$ at each thermocouple position:

$$\alpha(z) = \frac{q}{(T_{wi})_z - (T_{sat})_z} \tag{5}$$

where q is the inner wall heat flux to the fluid determined from the electric power supply to the test section after subtracting the heat loss. T_{wi} is the local inner wall temperature, which can be determined using the internal heat generation and radial heat conduction across the tube wall as given by:

$$T_{wi} = T_{wo} - \frac{q \cdot D_i}{4k}\left[\frac{(D_i/D_o)^2 - 2\ln(D_i/D_o) - 1}{1-(D_i/D_o)^2}\right] \tag{6}$$

T_{sat} is the local saturation temperature, deduced from the local fluid pressure assuming a linear pressure drop across the test section.

Thermodynamic Quality

An energy balance in each heated sub-section, which included the losses, was performed to determine the local specific enthalpy, h_i, at each thermocouple position as follows:

$$h_i = h_{i-1} + \frac{L_i}{\dot{m}L}(Q - \Delta Q) \tag{7}$$

The heat transfer, Q, is the total electric heat input, which is equal to the product of the voltage and the current applied directly to the test section. ΔQ is the heat loss determined using the loss coefficient obtained from single-phase test before each series of boiling tests, see Huo [26]. Therefore the local vapour quality can be calculated from the local specific enthalpy at each thermocouple position as:

$$x_i = \frac{h_i - h_l}{h_g - h_l} \tag{8}$$

where h_l and h_g are the specific enthalpy of saturated liquid and vapour, respectively.

Pressure Drop

This procedure was described in Huo et al. [27]. The pressure drop measured by the differential pressure transducer installed across the vertical test section is an overall contribution of three components: friction, acceleration and height, in which friction pressure drop was expected to be the major component.

$$\frac{dp}{dz} = \frac{dp_f}{dz} + \frac{dp_a}{dz} + \frac{dp_z}{dz} \tag{9}$$

where $\frac{dp_f}{dz}$ is the friction pressure gradient, $\frac{dp_a}{dz}$ the acceleration pressure gradient and $\frac{dp_z}{dz}$ the gravitational gradient. The friction pressure drop was calculated by subtracting the acceleration pressure drop and gravitational component from the measured value using the separated model, proposed by Lockhart and Martinelli in 1944, see Collier and Thome [28]. The acceleration component is given by Equation (10)

$$\frac{dp_a}{dz} = -G^2 \frac{d}{dz}\left(\frac{x^2}{\upsilon \rho_g} + \frac{(1-x)^2}{(1-\upsilon)\rho_l} \right) \tag{10}$$

and Equation (11) gives the gravitational component

$$\frac{dp_z}{dz} = g\left(\upsilon \rho_g + (1-\upsilon)\rho_l\right) \tag{11}$$

The local void fraction was calculated from the Lockhart-Martinelli multiplier using equation (12), see Collier and Thome [28].

$$\upsilon = 1 - \frac{1}{\phi} \tag{12}$$

The Lockhart-Martinelli multiplier is defined as [28]:

$$\phi^2 = \frac{(dp_f / dz)_{tp}}{(dp_f / dz)_l} = 1 + \frac{C}{X} + \frac{1}{X^2} \tag{13}$$

where $X^2 = (dp_f / dz)_l / (dp_f / dz)_g$ and C is a constant that depends on the liquid and vapour Reynolds number.

The five test sections 4.26, 2.88, 2.01, 1.1 and 0.52 mm in diameter had heated lengths of 500, 300, 211, 150 and 100 mm respectively; their corresponding roughness was 1.75, 1.54, 1.82, 1.28, 1.15 μm respectively. The mass flux was varied from 100 to 700 kg/m^{2}s and the heat flux from as low as 1.6 to 135 kW/m^2. Five different pressures were studied, namely 6, 8, 10, 12 and 14 bar. The maximum exit quality was 0.9.

The individual items of experimental equipment were carefully calibrated and single-phase tests were performed to verify the overall measurement accuracy of the test rig and its suitability for experiments at these small scales. The single-phase pressure drop and heat transfer results of the 4.26 mm tube were compared with well-known correlations. The agreement of the measured friction factor with the Blasius 1913 and Haaland 1983 correlations (cited in Massey and Ward-Smith [29]) was within 5%. The average Nusselt number was compared with the Dittus-Boelter [30] and the Petukhov [31] correlations with excellent agreement (within the experimental uncertainty). However, the measured friction factor of the 0.52 mm tube was more than twice the value given by the correlation of Blasius and Haaland (with relative roughness 0.00115/0.52) in the turbulent region and (16/Re) in the laminar region. The single-phase heat transfer results of this tube compared well with the Gnielinski [32] and the modified Gnielinski [33], which allows for a transition region and developing effects. They also compared well with the Adams et al. [34] correlation, which is a modification of the Gnielinski relation and accounts for the small diameter effects. In the laminar region (Reynolds number less than 2500) the Nusselt number was in good agreement with Choi et al. [35], see Shiferaw et al. [36] for further details.

The reproducibility of the experiments carried out in the 4.26-1.10 mm tubes was excellent and within the experimental uncertainty in the region where dryout did not occur. The region with partial dryout (decreasing heat transfer coefficient – see Section 5) is associated with temperature fluctuations and may indicate some higher degree of deviation between experiments performed at different times but still within reasonable limits. The reproducibility of the experiments in the 0.52 mm tube was acceptable in the lower range of heat flux (<11 kW/m^2), had significant differences in the intermediate region (11-18 kW/m^2) and then got progressively better, i.e. at q > 37 kW/m^2 it was within the uncertainty limits, see Shiferaw [37]. The experimental procedure for the tube was identical as for the other tubes. Therefore there is a *possibility* that this lack of reproducibility for a certain range is due to sparse and / or unstable nucleation sites. This will be examined further and will include hysteresis experiments. The uncertainty in the temperature measurements was about 0.16 K. The uncertainty in the pressure and differential pressure was 0.15-0.27% and 0.27-30% respectively. The two coriolis meters (see figure 6) provided mass flow measurements with a negligible uncertainty of 0.44%. The uncertainty in the heat flux measurements was 0.5 to 1.5 % and the propagated uncertainty in the heat transfer coefficient was 6 to 12.5%.

3. FLOW PATTERNS

Classification of the flow patterns in small to micro diameter passages is yet to be agreed upon by the research community. The particular flow regimes that prevail at given values of liquid and vapour velocities depend up on the relative magnitude and interaction of gravity, shear stress and inertia, surface tension and turbulent forces (Coleman and Garimella [38]. It is generally accepted that the flow regimes in these passages are considerably different than those observed in large size tubes (typically bubbly, slug, churn and annular flows in vertical tubes with additional regimes such as stratified and wavy flows in inclined or horizontal tubes). Differences due to the increasing dominance of surface tension as the diameter diminishes include the absence of stratified flow and the independence of the flow regimes of channel orientation. In

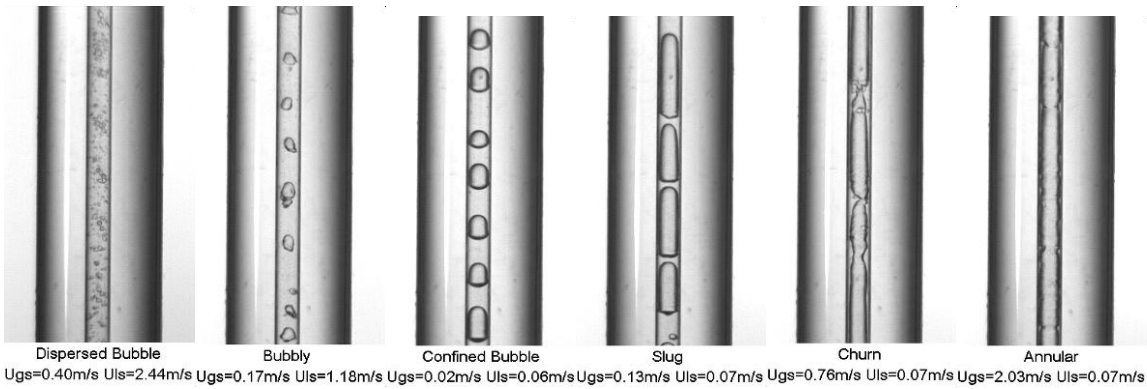

(a)

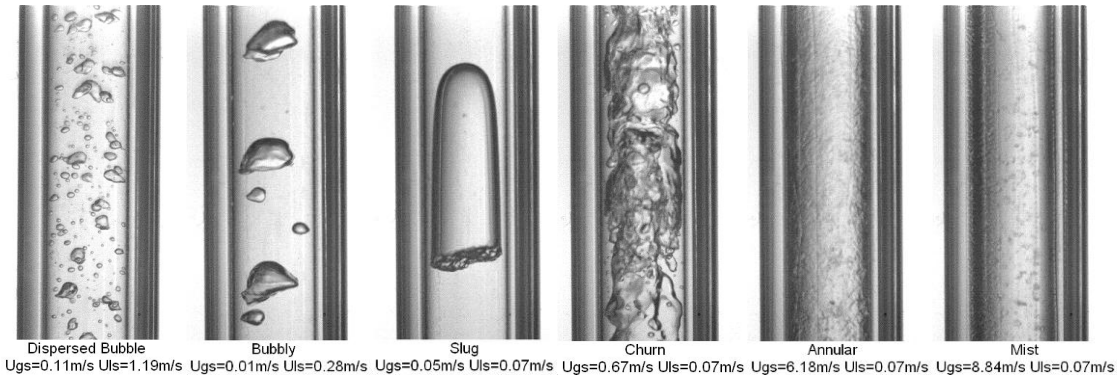

(b)

Figure 8. Flow patterns for R134a at 10 bar pressure: (a) d = 1.10 mm, (b) d = 4.26 mm, Chen et al. [25].

some early studies some researchers reported a very detailed flow classification. For example, Oya [39] noted simple bubble, granular- lumpy bubble, simple slug, fish-scale type slug, piston, long piston, froth, and annular flow in experiments with air/water. However, most of them identified a smaller number of patterns. Table 2 lists some of the past research in this area and is indicative of the flow regimes identified by the various research groups and the need to converge into an agreed classification of the pertinent flows regimes that will also help the attempts to model two-phase heat transfer and pressure drop in these passages. Classification of the prevailing flow regimes can be difficult due to experimental uncertainty and the subjectivity of the observer. However, the most commonly identified flow patterns are: bubbly, slug flow, churn flow and annular flow. Some researchers did not differentiate between dispersed bubble and bubbly flow.

A detailed and systematic study on flow patterns in vertical two-phase flow was performed at Brunel University and reported by Chen et al. [25, 40]. The research used the same experimental facility described in this paper, R134a as the working fluid and covered the range of tube diameters 4.26, 2.88, 2.01 and 1.1 mm for a system pressure of 6-14 bar. Typical flow patterns observed in this study are included in Table 1 and are depicted in figure 8 for the 4.26 and 1.1 mm tubes. The flow patterns in the larger tubes of this study (dispersed bubble, bubble, slug, churn, annular and mist flow) were similar to those expected in vertical two-phase flow in macro tubes. However, examination of the 1.1 mm tube results indicate significant differences, namely: the appearance of confined bubble flow, a slimmer vapour slug as well as a less chaotic liquid-vapour interface in the churn flow. These "small tube characteristics" (Chen et al. [40]) were first apparent in the 2.01 mm tube and became clearly established in the 1.1 mm tube.

Table 2 includes recent studies with smaller tubes (< 1 mm) where further differences were reported. Zhao and Bi [47] reported that dispersed bubble was not present in the smallest of their triangular channels (d_h= 0.866 mm). Serizawa et al. [48] reported the following flow patterns: bubbly, slug, liquid ring flow and liquid lump flow. The appearance of a symmetrical liquid ring with long gas slugs passing in the middle was identified as the liquid ring flow. Serizawa et al. assumed that the liquid ring flow could develop from slug flow when the gas slug velocity is too high and the liquid slug is too short to form a stable liquid bridge between consecutive gas slugs. They described liquid lump flow as follows: "the high-speed core gas entrains the liquid phase and liquid lumps are sliding on the wall". Liquid lump flow followed the liquid ring flow when the gas flow rate was increased.

Kawahara et al. [49] in their introduction mentioned the differences reported in two-phase flow pattern maps (as well as void fraction and pressure drop measurements) when the channel hydraulic diameter changed from 10 to 1 mm. The researchers went on to note that "for another order-of-magnitude reduction in the channel diameter from ~1 mm to 100 μm further changes in the two-phase flow characteristics are expected". They studied two-phase flow
in a circular transparent channel made of fused silica of internal diameter 0.1 mm and 64.5 mm long. The flow patterns observed were mainly intermittent and semi-annular flows. They continued to classify their patterns into five distinct groups, i.e. liquid alone, and gas core with
(i) smooth-thin liquid film, (ii) smooth-thick liquid film,

Table 2. Flow patterns reported in past studies for small diameter tubes and channels

Reference	Passage size and fluid	Flow patterns
Barnea et al. [41]	4 – 12 mm tubes Air-water	Dispersed bubble, elongated bubble, slug, churn and annular
Damianides and Westwater [42]	1-5 mm tubes Air-water	Dispersed bubble, bubbly, plug, slug, pseudo slug, wavy and annular
Mishima and Hibiki [43]	1 – 4 mm tubes Air-water	Bubbly, slug, churn, annular and annular-mist flow
Kew and Cornwell [44]	1.39 and 3.69 mm tubes R141b flow boiling	Isolated bubble, confined bubble and slug/annular flow
Lin et al. [45]	0.5-4.0mm tubes Air -water	Bubbly, confined bubble, slug, churn and annular
Triplett et al. [46]	1.1 and 1.45 mm tube 1.097 and 1.49 mm semi-triangular microchannel Air-water	Bubbly, slug, aerated slug-churn, slug-annular, annular
Zhao and Bi [47]	Triangular channels 2.886, 1.443, 0.866 mm Air-water	Dispersed bubble, slug, churn, annular Dispersed flow was not present in the d_h=0.866 channel.
Serizawa et al. [48]	0.02, 0.025, 0.05 and 0.1 mm tubes Air-water and steam-water	Bubbly, slug, liquid ring flow, liquid lump flow. Lump flow was not observed when using steam-water.
Kawahara et al. [49]	0.1 mm tube Nitrogen-deionised water	Liquid alone, and gas core with (i) smooth-thin liquid film, (ii) smooth-thick liquid film, (iii) ring-shaped liquid film and (iv) deformed interface. (Bubbly and churn flows were absent)
Chung and Kawaji [50]	0.05 to 0.53 mm tubes Nitrogen-water	Bubbly, churn, gas core flow with smooth thin liquid film, gas core flow with wavy liquid film (liquid ring flow), slug-annular, annular. Churn observed only in 0.25 and 0.53 mm at certain conditions.
Chen et al. [40]	1.1, 2.01, 2.88 and 4.26 mm tubes R134a	Dispersed bubble, bubbly, slug, churn, annular and mist flow. Confined flow was observed in the d=2.01 and 1.1 mm tubes.
Xiong and Chung [51]	Triangular channels 0.209, 0.412 and 0.622 mm Nitrogen-water	Bubbly, slug, slug-ring (liquid-ring flow), dispersed-churn flow and annular flows. Dispersed-churn flows were absent in the d_h=0.209 mm channel.
Revellin and Thome [52]	0.51 and 0.8 mm tubes	Isolated bubble, Coalescing bubble and annular flow

(iii) ring-shaped liquid film and (iv) deformed interface. They did not observe bubbly or churn flow patterns and they attributed this to the laminar nature of the liquid flow in their microchannel. Recently, Xiong and Chung [51] studied adiabatic gas-liquid flow patterns using nitrogen and water in rectangular microchannels and observed four different flow patterns: bubbly, slug flow, slug-ring flow (liquid-ring flow), dispersed-churn flow, and annular flow in the 0.412 and 0.622 mm microchannels. Dispersed and churn flows were absent in their 0.209 mm channel. Revellin and Thome [52] identified three main flow patterns, i.e. the isolated bubble regime (bubbly flow and short slugs) the coalescing bubble regime (slug flow is the main flow with some of the bubbles coalescing together to form a longer slug) and the annular regime. They stated that churn flow is a transition from coalescing bubble to annular flow.

Flow visualization experiments at the exit of the test section, with the current test facility in a 0.52 mm tube, were performed as part of a heat transfer study [53]. The flow patterns noted included: bubbly flow, confined bubble flow and wavy film flow that led to annular flow, see figure 9. Dispersed bubble flow was not seen in this tube. The wavy film flow was developed from confined flow with increasing heat flux; as the heat flux increases confined bubbles grow in length and become elongated and with a further increase, the liquid slug is pushed onto the downstream bubble. This results in bubble coalescence similar to the observations of Revellin et al. [32].

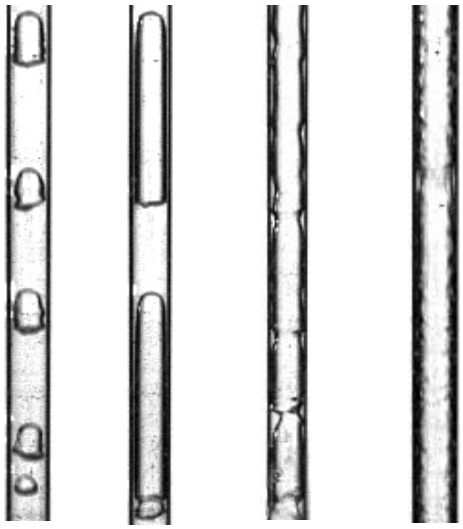

1 2 3 4

No	q (kW/m^2)	U_{gs} (m/s)	U_{ls} (m/s)
1	9.5	0.92	0.31
2	12.8	1.33	0.29
4	17.9	1.97	0.27
9	55.5	7.06	0.11

Figure 9. Flow pattern in of 0.52 mm tube at 400 kg/m^{2}s and 8 bar.

The effect of diameter on the flow pattern transition boundaries was studied by Chen et al. [40] and discussed also in Karayiannis et al. [53] for tube diameters 4.26, 2.88, 2.01 and 1.1 mm. The diameter was found to influence the dispersed bubble-bubbly, slug-churn and churn-annular transition boundaries. There was no effect noted for the dispersed bubble-churn and bubbly-slug boundaries. The slug-churn and churn-annular boundaries were found to be weakly dependent on the superficial liquid velocity and strongly dependent on the superficial vapour velocity.

Ravellin and Thome [52] proposed flow pattern transition boundaries, which provide the quality at transition in terms of the Reynolds, Boiling and Weber numbers for the isolated bubble-coalescing flow transition and in terms of the Reynolds and Weber number for the coalescing-annular transition boundaries. Ullmann and Brauner [5] examined the effect of diameter on the mechanisms leading to flow pattern changes and suggested mechanistic models for the transitions. Chen et al. [54, 55] following their analysis, proposed models and correlations for the transition boundaries of dispersed bubble-bubbly, bubbly-slug, slug-churn and churn–annular transition boundaries.

4. PRESSURE DROP

Heat transfer models must be solved in parallel with a pressure drop model to predict the local saturation temperature. Models and correlations are generally adaptations of methods for large channels, particularly homogeneous flow (same velocity for both phases) and the separated flow methods of Martinelli and Nelson [56] and Chisholm [57]. In most cases the friction loss was dominant compared to acceleration and hydrostatic losses. In 2000, Tran et al. [58] studied pressure drop in small channels and tubes, in order to determine if large-tube correlations could be used to predict two-phase pressure drop of refrigerants in channels with hydraulic diameter 2.4-2.9 mm. Five state-of-the-art large-tube correlations failed to predict the pressure drop for flow boiling in the small channels for all test conditions. The researchers attributed the divergence to the confined bubble flow patterns that can exist over larger ranges of void fraction in the small channels. Tran et al. proposed a new correlation for the pressure drop, neglecting the acceleration component. However, earlier, Kureta [59] found that the acceleration loss was comparable to the friction loss under certain conditions for water boiling in 2 – 6 mm diameter tubes. Recently, Ribatski et al. [60] compared 12 prediction methods with a large database for adiabatic and boiling flow in microchannels. The best-performing methods could only predict 50% of the data within an error band of ± 30%, similar to the performance of the best heat transfer methods. They also noted considerable differences between data sets for similar conditions produced at different laboratories, suggesting that important variables were not being controlled. These may include surface roughness and the inlet and outlet connections, which may influence flow instabilities. (The data set included data for single channels and parallel groups). Wen and Kenning [61] found that the homogeneous model predicted satisfactorily the time-averaged pressure gradient for water boiling at atmospheric pressure in a rectangular 2 x 1 mm channel. Unusually, they measured the pressure differences across separate sections of the channel, not just between inlet and outlet headers. They found that the greatest variability occurred in the entrance region, probably associated with variations in the position of initial bubble nucleation dependent on the availability of nucleation sites. Huo et al. [27] presented experimental results for pressure drop for R134a boiling in vertical 2.01 and 4.26 mm diameter tubes at 8-14 bar for the same wide range of heat fluxes and flow rates as their heat transfer data and using the current experimental facility. There were only small variations in the internal roughness of the tubes (1.82 and 1.75 μm for the 2.01 and 4.26 mm tubes respectively). The incoming liquid flow was fully-developed and the outgoing flow pattern was undisturbed. They reported that the pressure gradient in the smaller tube was approximately three times higher than in the larger tube. They compared their results with the correlations of Tran et al. [58] and Yu et al. [62], Warrier at al. [63], Lee and Lee [64] and Qu and Mudawar [65] and the correlation of Chisholm [66]. The Chisholm correlation was the only one that predicted their results for both tubes mostly within 30% - the agreement was similar for both tubes, which suggests that there is no diameter effect on this correlation down to 2 mm. The agreement with the other correlations was much worse.

From the above survey, it can be seen that methods for predicting the time-averaged two-phase pressure drop in large tubes are not reliable for small diameter passages. There is

disagreement about the significance of the acceleration pressure loss compared to the friction loss. The time-averaged acceleration pressure loss is calculated and instantaneous accelerations, which may be much larger, particularly at low pressures, are not considered. The currently available experimental data for small/micro tubes are scarce, especially for a substantial range of variables. In some cases, they were not obtained with specified and well controlled important variables and may include the losses in the inlet and outlet plena.

Pressure drop results

In the present experiments, the pressure drop was found to increase almost linearly with heat flux, although it should be noted that at high heat flux values, it could decrease due to the occurrence of dryout at high exit qualities, i.e. single-phase vapour flow may exist for a significant part of the tube. The pressure drop increased with mass flux and decreased with system pressure, see also Huo et al. [27]. The latter effect is due to the decrease in the ratio of the liquid to vapour density as the pressure increases. The total measured two phase pressure drop results for the five tubes of diameter 4.26 to 0.52 mm are plotted as a function of exit quality in figure 10 at 8 bar system pressure and 400 kg/m^{2}s mass flux. The pressure drop gradient is used due to the fact that the pressure drop lengths of the tubes are different (521, 321, 233, 165 and 108 mm for the 4.26, 2.88, 2.01, 1.1, and 0.52 mm respectively). As shown in the figure, the pressure drop gradient generally increases with decreasing tube diameter. However, at high exit quality, the effect is less clear for the three larger tubes (4.26 – 2.01 mm). The pressure gradient increases significantly as the tube diameter decreases from 2.01 to 1.1 mm, while the two phase pressure gradient of the smallest tube (0.52 mm) is much higher. As mentioned above, the single phase pressure drop of this tube was also more than twice the value from the classical correlations of Blasius and Haaland in the turbulent region and (16/Re) in the laminar region. Preliminary results of surface roughness measurements carried out at the Institute for Thermodynamics of the University of Hannover indicated non-uniformity in the channel cross-section. This could explain the behaviour of the 0.52 mm tube. This is currently under further investigation. It confirms the importance of surface characteristics at these small sizes. It is also indicative of the possible differences between laboratories since there is no standard method of confirming the internal surface conditions in commercially available products used in research.

The contribution of the three different pressure drop components, i.e. gravitational, acceleration and friction pressure drop, on the measured total two phase pressure drop were analysed for all the tubes. Figure 11 depicts a typical example for the 1.1 mm tube at a mass flux of 400 kg/m^{2}s and 8 bar pressure with the actual value of the friction pressure drop also plotted on the graph. The acceleration and gravitational pressure drops were calculated using the separated flow model, see Section 2. The frictional component is by far the greatest. But, as seen in the figure, the acceleration pressure drop contribution, which was sometimes ignored (Tran et al. [58]) or included (Kureta et al. [59]) become increasingly important as the exit quality increases, reaching a value slightly above 30 % at exit quality of ~ 0.86. On the other hand the gravitational and frictional pressure drop contributions gradually decrease with exit quality.

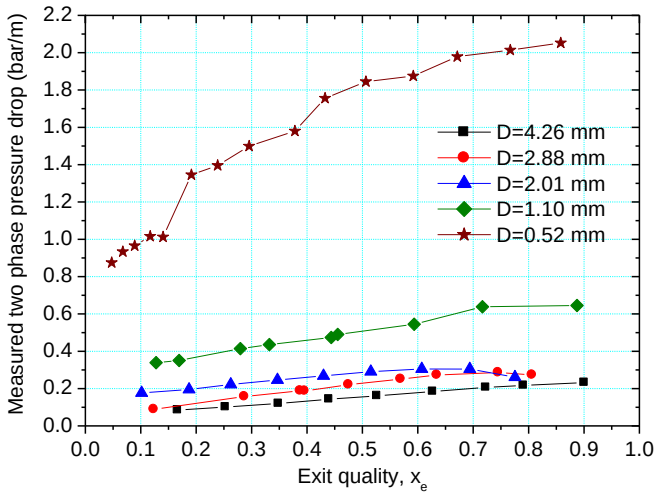

Figure 10. Effect of tube internal diameter on two phase total pressure drop gradient as a function of exit quality at 8 bar system pressure and 400 kg/m^{2}s mass flux.

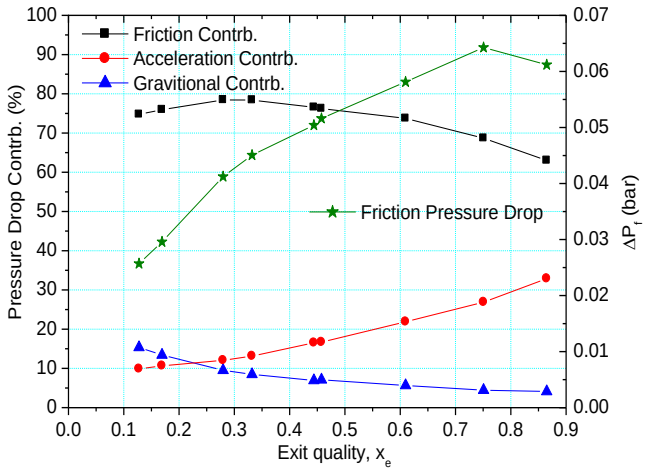

Figure 11. Percentage contribution of the three pressure drop components to the total measured value and the calculated friction pressure drop component at a mass flux of 400 kg/m^{2}s and 8 bar system pressure for the 1.1 mm diameter tube.

Comparisons of pressure drop results with existing correlations

The results of the measured pressure drop were compared with various models and correlations including the homogeneous model, the separated model of Lockhart and Martinelli (see [28]), Chisholm [66], Tran et al. [58], Mishima and Hibiki [43] and Muller-Steinhagen and Heck [67]. A summary of the comparative performance of the different models and correlations is presented in Table A1, in the Appendix using the Mean Absolute Error (MAE) and percentage of data within ±30% (β). The comparative results indicated that the larger tube (4.26 mm) data are predicted well by the separated flow model of Lockhart-Martinelli and that of Chisholm. However, as the tube diameter decreases from 4.26 mm to 1.1 mm, the Lockhart-Martinelli and Chisholm correlations tend to over-predict the data and the MAE and β change from 14/90 and 15.1/91 to 25/75 and 27/74 respectively. Figure 12 shows the comparison of the 2.88 mm tube data with the Chisholm correlation.

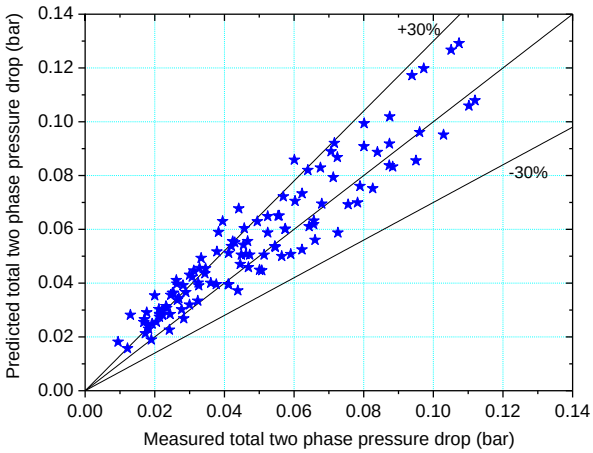

Figure 12. Comparison with the Chisholm [66] pressure drop correlation for the 2.88 mm tube.

The homogeneous model generally under-predicts the data for all tubes. The Mishima-Hibiki [43] correlation predicts the data of the 4.26 mm tube fairly well (16/92) but progressively underpredicts the data; this difference being significant for the 1.1 mm tube. The Tran et al. [58] correlation under-predicts our data significantly. Muller-Steinhagen and Heck [67] predicted the two-phase frictional component and this was compared with the current data. The correlation underpredicted the data significantly (most of the data by more that 30%). In this comparison the acceleration and gravitational components were obtained using the homogeneous model as also carried out by Muller-Steinhagen and Heck. The comparison did not improve when these were calculated using the separated flow model of Lockhart-Martinelli. The 0.52 mm tube data are not predicted well by any of the prediction methods. As discussed above, surface roughness and channel cross-section non-uniformity may be different than the other tubes as shown by the preliminary surface roughness measurement results. The comparative study concluded that separated flow model and the correlation of Chisholm predicted the current data better than the other models/correlations. However, overall, among the prediction methods listed above, there was no single model or correlation that predicted the data for all the tubes with similar or near similar accuracy. This is indicative that further work and a better model or correlation is needed to predict the pressure drop at these sizes and capture the diameter effect correctly.

5. HEAT TRANSFER RESULTS

Discussion of the experimental heat transfer results and their dependence on mass flux, system pressure and tube diameter for the five tubes (4.26- 0.52 mm) were presented in Karayiannis et al. [53]. They reported that in the 4.26 and 2.88 mm diameter tubes, the heat transfer coefficient increases with heat flux and system pressure, but did not change with vapour quality when the quality was less than about 40% to 50%, for low heat flux. The boundary moves to 20% - 30% for the 2.01 and 1.10 mm diameter tubes. The actual quality values depend also on the heat flux. In this region, there is no significant difference in the magnitude of the heat transfer coefficient of the 4.26 and 2.88 mm tubes. However, considering only the uniform heat transfer coefficient region, there is an increase of 15% and 35% when the tube diameter is reduced to 2.01 and 1.10 mm respectively.

Typical heat transfer results at different heat flux as a function of quality and axial position for the 1.10 mm tube and 0.52 mm are presented in this paper at a mass flux of 300 kg/m^{2}s and 6 bar pressure to clarify and facilitate further discussion. As seen in figure 13 (a), the local heat transfer coefficient increases with increasing heat flux and at low heat flux the value is approximately uniform. At high heat flux (q > 51 kW/m^2), there is a sharp decrease in heat transfer coefficient with quality after a quality of about 0.35. The heat transfer coefficient lines merge indicating no significant effect of heat flux in this region. The temperature of the wall in this part was highly unstable which may indicate partial (intermittent) dry out, Shiferaw et al. [68]. As also seen in the figure, the effect of heat flux on the heat transfer coefficient reverses after q = 69 kW/m^2 for x < 0.32, i.e. the heat transfer coefficient for q=86.1 and 103.7 kW/m^2 is lower that that for q=69.6 kW/m^2. Similar trends were observed in the 2.01, 2.88 and 4.26 mm tubes, see for example Karayiannis et al. [53] for different flow rates and pressures.

Figure 13 (b) is a plot of the heat transfer coefficient versus location along the flow direction. As seen in the figure, there is a decrease in the local value from the first to the second measuring point, which is more evident at high heat flux. This could be related to the high heat transfer coefficient in the subcooled boiling regime. The fact that the patterns of changes in heat transfer rates at different heat fluxes correspond to particular measuring locations,

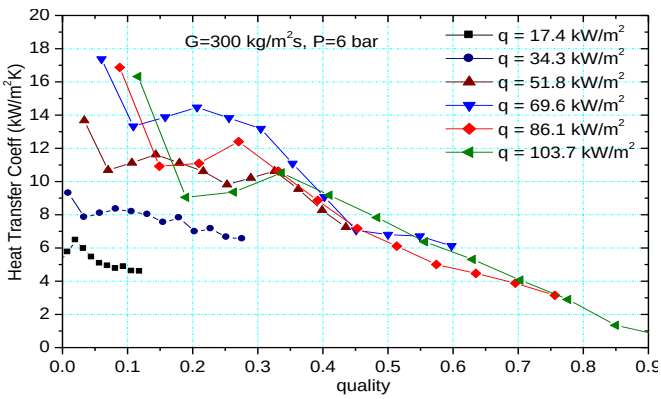

(a)

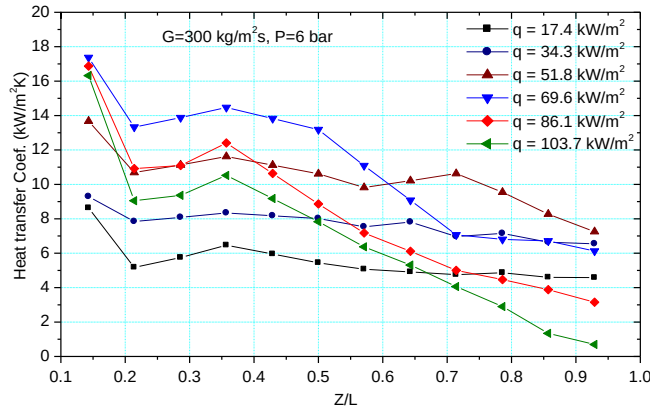

(b)

Figure 13. Local time-averaged heat transfer coefficient, for D = 1.1 mm, G = 300 kg/m^{2}s and P = 6 bar, as a function of: (a) local quality, (b) axial position.

e.g. peaks at or near the 4th measuring location, may indicate the effect of surface variations since systematic measuring errors are ruled out by the disappearance of such variation in single-phase tests that were always performed prior to the flow boiling tests.

The heat transfer results of the smallest diameter tube (0.52 mm) demonstrated different characteristics than the rest of the tubes, see also [53]. As seen in figure 14 (a), the dependence of the heat transfer coefficient on quality, heat flux and mass flux change sharply in character at a threshold value of heat flux, 12.5 kW/m^2 < q < 14.8 kw/m^2 in this case. In the low heat flux region, there is no significant effect of heat flux but the heat transfer coefficient decreases (at low mass flux and pressure) or remains constant (at higher mass flux and pressure), then increases gradually with quality, see also [53]. When the heat flux is increased to 14.8 kW/m^2, the second group exhibit varying trends. These correspond to an increase, decrease and gradual increase of heat transfer coefficient with quality (zones I, II and III respectively included in the figure for clarity). The region of heat transfer coefficient which is independent of heat flux and decreases with quality associated with dryout seen in the larger tubes of our study was not observed in this tube. Looking only at the heat transfer

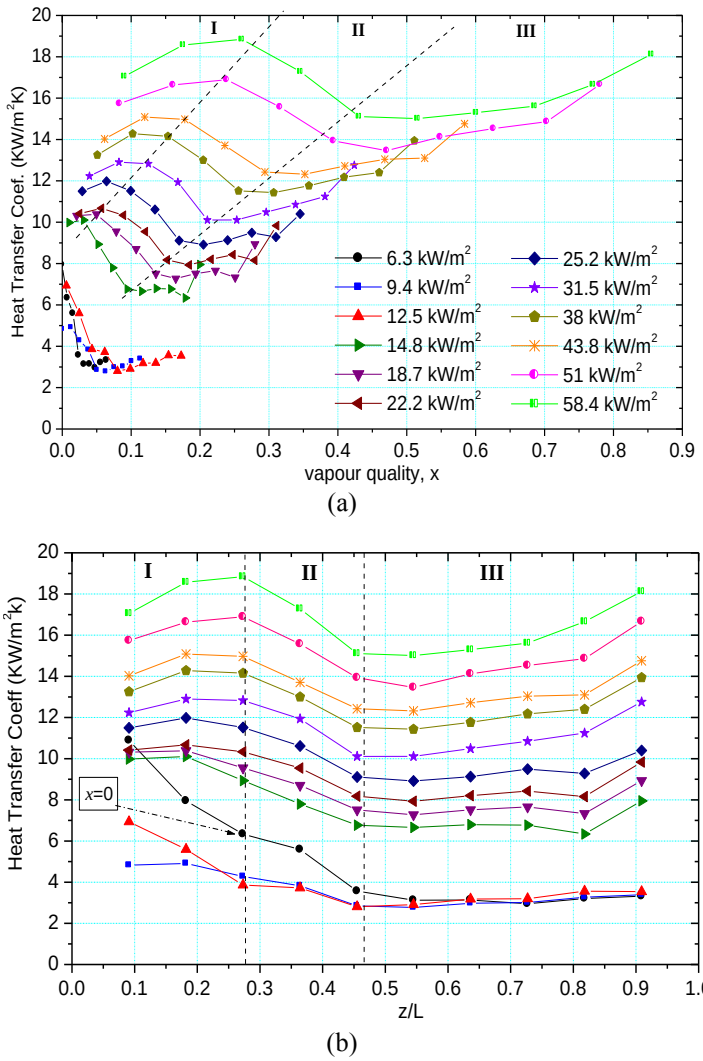

Figure 14. Local time-averaged heat transfer coefficient, for D=2.88 mm, G = 300 kg/m^{2}s and P = 6 bar, as a function of (a) local quality, (b) axial position, [53].

coefficient versus quality plot, one could suggest that the results are more similar to the macro-tube patterns, see figure 1: the pattern of separate lines of nearly constant heat transfer coefficient with quality at low quality merging with a single line of *increasing* heat transfer coefficient at higher quality. However, the variation in the coefficient with non-dimensional axial length, figure 14 (b), suggest a different interpretation. A similar pattern of changes for all values of heat flux greater than 14.8 kW/m^2, with a value that increases with heat flux almost uniformly, is observed. Unlike figure 14 (a), there is a clear effect of heat flux for all the regions. At the lowest heat flux of 6.3 kW/m^2, the heat transfer coefficient drops with axial distance near the inlet. This could be due to the effect of inlet subcooling, i.e. the heat flux is so low in this case that saturation commences far into the tube at z/L ~ 0.27 (identified on the figure with x=0). Therefore, the large heat transfer coefficient at the inlet may be caused by the onset of subcooled boiling. Again, the fact that the patterns of changes at various values of heat flux are associated with axial locations may indicate the importance of surface characteristics. In contrast with the larger tubes of this study, a higher wall superheat was required to initiate boiling, see [53]. This could be related to the availability of active nucleation sites which could be very small due to the small internal surface area of this tube. The threshold heat flux that separates the clearly different effect of heat flux on the heat transfer coefficient demonstrated random variation with mass flux and pressure. However, it seems to coincide, at least in some cases, with the appearance of the wavy film flow pattern seen in figure 9.

Comparison with existing correlations

Correlations for small/micro diameter channels usually followed traditional approaches based on research in macro-tubes and the existence of nucleate boiling and forced convection heat transfer, see section 1. Superposition of these components provides the overall two-phase flow heat transfer rates. This can be done in a simple additive (first suggested by Rohsenhow [69]) or in an asymptotic approach (Kutateladze [70]). Shah [71] also recommended selecting the greater of the two components. Dimensionless factors were introduced by Chen [72], i.e. the suppression factor and the enhancement factor to allow for the reduction of superheat due to forced convection compared to that in pool boiling and the heat transfer increase due to vapour flow respectively. Correlations such as those of Gungor and Winterton [73] and Liu and Winterton [74] follow this approach. A basic more recent improvement in correlating for small-micro tubes is the inclusion of laminar flows in, for example, in the work for Zhang et al. [75] and Saitoh et al. [76], which as mentioned in Section 1, must be important for small/micro passages. A different more simple approach involved the use of a data bank to obtain statistical correlations based on the Boiling, the Weber and the Reynolds numbers, such as the work of Lazarek and Black [77] and Tran et al. [78].

The heat transfer coefficients obtained for all the tubes were compared with some of the existing correlations. The data used excluded the heat transfer coefficient values where dryout occurred, i.e. used data in the region where the heat transfer coefficient was independent of quality and dependent of heat flux. This was as follows: 4.26 mm tube, x<0.5; 2.88 mm tube, x<0.48; 2.01 mm tube, x<0.32 and for the 1.10 mm tube, x<0.3. All the data were used for the 0.52

mm tube. The selected correlations include Lazarek and Black [77], Gungor and Winterton [73], Liu and Winterton [74], Tran et al. [78], Zhang et al. [75], Saitoh et al. [76] and Kandlikar and Balasubramanian [79], All the above correlations except that of Saitoh et al. did not consider dryout and post dryout data. Table A2 in the Appendix gives the mean average error and the percentage of data within ± 30% obtained in these comparisons. The Lazarek and Black correlation under-predicted all our data consistently. The disagreement was less for the 2.88 mm tube possibly since their correlation was based on a 3.1 mm tube. The comparison with the Tran et al. correlation, which is similar to the above, demonstrated better agreement with the 4.26 and 2.88 mm tube data than that of Lazarek and Black. However, the agreement deteriorated progressively (underpredicted the data) as the diameter was reduced (MAE/β of 15/100 at D=4.26 mm to 52.5/0 and 73.5/1.5 for D=1.10 and 0.52 mm respectively). The Gungor and Winterton correlation predicted our data fairly well, with the exception of the 0.52 mm data. The later correlation of Liu and Winterton was not as successful and underpredicted our data consistently by about 30%, see Table A2 for corresponding MAE and β values. The Kandlikar and Balasubramanian correlation, which was based on an earlier version by Kandlikar [80] to allow for laminar flows in small passages proved to be a fairly poor comparison; there was a significant scatter and the agreement got progressively worse as the diameter was reduced. The Zhang et al. correlation employed the Foster and Zuber [81] term for the nucleate boiling part. When this correlation was compared with the current data the results were not satisfactory at all. The data were significantly underpredicted and MAE and β were very high and nearly zero respectively, see Table A2. We replaced the Foster and Zuber term with the correlation proposed by Cooper [82] for the nucleate term. In this case the comparison was significantly improved with the MAE being less that 20 and β greater than 86 for the 4.26 to 1.10 mm tubes, see figure 15 for the comparison with the 2.88 mm tube data. The correlation of Saitoh et al. under-predicted the data by more than 30%, a disagreement which is higher that the similar-basis correlations of Gungor and Winterton and Zhang et al. As indicated above, the correlations above offer only limited success in prediction the current data although the agreement with the Gungor and Winterton [73] and the modified Zhang et al. [75] correlation is better. The data of the smaller 0.52 mm tube were very poorly predicted by all correlations including those of Gungor and Winterton and Zhang et al. The experimental procedure followed for this tube was identical to that followed for the rest of the tubes of this study with a careful commissioning and validation of the rig using single-phase tests. As discussed above in relation with the pressure drop results, this tube may have such surface characteristics that at this size introduce both a higher pressure drop than expected and possible different heat transfer characteristics. Experiments are currently under way to re-examine this data along with a detailed evaluation of the surface structure of this tube. This research will include a tube from the same length of tube that the 0.52 mm tube was cut and possibly a second similar size tube from a different manufacturer.

6. MECHANISTIC MODELS

1-D Modelling

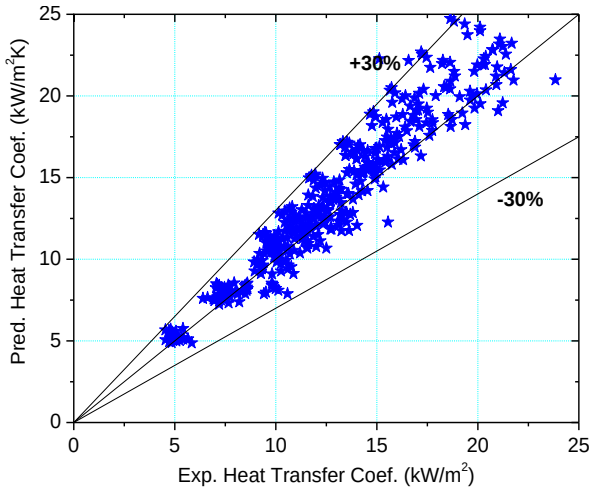

Figure 15. Comparison with the Zhang et al [75] correlation using the Cooper [82] correlation for the nucleate boiling term for the 2.88 mm diameter tube.

Correlations of heat transfer and pressure drop in small channels are guided by physically-based models that in turn depend on localized experimental data for validation and, in the case of 1-D models, for input. Mechanistic models with no empirical input are still far from replacing correlations. Models for flow boiling at low quality in large tubes containing many bubbles at present require some spatio-temporal averaging over groups of bubbles. Modelling at high quality, after bubbles have agglomerated into annular flow, faces different difficulties of wavy, turbulent liquid films and the entrainment of droplets in the turbulent vapour core.

As the channel cross-section is reduced, it becomes feasible to model individually all the bubbles in the confined bubble regime, which, from flow maps based on observations such as Fig. 8, appears to persist to higher qualities in smaller channels. Fully 3-D modelling with the requisite resolution of heat transfer across thin liquid films would be extremely demanding. An alternative is to use 1-D modelling dependent on a small number of simplified sub-models and correlations based on localised flow visualization and experimental data, some of which must be reserved for independent validation. Flow observation combined with local measurements is simpler in channels of rectangular cross-section with an adiabatic window on one side but modelling is simpler for a circular cross-section.

Kew and Cornwell developed a 1-D model for the pressure fluctuations in confined bubble flow, assuming a boundary condition of uniform wall heat flux [83]. This thermal condition was used in the heat transfer model of Jacobi and Thome [84], further developed into the 3 – zone model [22,23] with which they challenged the conventional large-tube interpretation of flow boiling as dominated either by nucleate boiling or convective boiling. The model assumed that the effect of the pressure fluctuations was negligible. The validity of this assumption will be discussed under Pressure Fluctuations below. The comparison of the Thome et al. 3- zone model with experimental data from the present study is also be discussed. Faghri and colleagues [7, 85, 86] developed a model for a pulsating heat pipe operating between regions of uniformly high and low wall temperature that necessarily included the effects of pressure

pulsations, since these drove the motion. Kenning et al. [10] developed a model for the pressure changes induced by the growth of a single confined bubble in an initially uniformly superheated tube with no inlet flow and transient conduction in the liquid film and the wall. Improvements to the 3-zone model in the light of these other models will be discussed in the last part of this Section. Models for heat transfer in the annular flow regime in capillary tubes, e.g. [87, 88], including the explosive transition from liquid flow to annular flow without an intervening bubble flow regime [89] will not be examined in this paper.

Pressure fluctuations

The Kew and Cornwell model for pressure fluctuations [83] assumes that a confined bubble grows from an initial length approximately equal to the tube diameter D by evaporation of a liquid film of negligible thickness over its entire instantaneous length L_b (t) due to the wall heat flux q, causing exponential growth with time (assuming constant saturated vapour density ρ_v):

$$L_b = De^{ft}, \quad f = \left[4q/\rho_v\, h_{\lg} D\right] \qquad d^2L_b/dt^2 = f^2De^{ft} = f^2L_b \tag{14}$$

The pressure difference required to accelerate the liquid slug of length L_l ahead of the bubble is

$$\Delta p = \rho_l L_l f^2 L_b \tag{15}$$

A correction for the change in vapour density with pressure was given. They found that the pressure difference required to accelerate a liquid slug 10 mm long was consistent with the measured fluctuations in *total* pressure drop of amplitude ~ 30 kPa at 2 Hz for water at near-atmospheric pressure boiling in a 2.87 mm diameter tube at 300 kg/m^2, 110 kW/m^2. Video observations combined with pressure measurements at intermediate stations [15] for water in a 2 x 1 mm channel confirmed that pressure pulses of this order of magnitude travelled with individual liquid slugs. Zhang et al. [12] observed pressure fluctuations exceeding 1 bar at 3-10 Hz for water boiling in a 0.25 x 0.1 mm diameter silicon channel.

By a small extension of the basic model, the initial mass of the liquid slug is given by the product of the mass flux G and the period between confined bubbles τ, decreasing to $(1\text{-}x)G\tau$ at quality x, if the superheating of the liquid slug implicit in the model is disregarded. The combined length of all bubbles up to x, which determines the acceleration of the liquid slug, is somewhat less than the heated length $xDGh_{lg}$ / $4q$. The maximum pressure difference across one slug, occurring at x = 0.5, is then :

$$\Delta p_{\max} = G\tau\, f^2 DGh_{\lg}/16q = G^2\tau q/\rho_g^2 h_{\lg} D \tag{16}$$

Values predicted by this simple model are shown in Table 3 for water and R134a at the same conditions and demonstrate a large decrease with increasing pressure. Δp would be increased by viscous resistance but reduced by the leakage past the bubbles of liquid films of finite thickness. The values for water at 1 bar are much larger than the measured values in a 2 x 1 mm channel [15], when scaled to the experimental conditions, in which the measured axial acceleration of the liquid slug and the pressure pulse were lower than predicted by equation (16). It was shown in [10] for water at 1 bar in glass capillary tubes at G = 0 that the right magnitude of pressure pulse could be modelled by including the effect of finite liquid film thickness and the feedback between pressure changes and the superheat driving bubble growth by evaporation, but steady-flow expressions for frictional resistance were inaccurate. Brutin and Tadrist, in flow boiling experiments with variable inlet compressibility with n-pentane [17,18], showed that at low compressibility the magnitude of pressure fluctuations decreased with increasing Reynolds number of the incoming laminar liquid flow. This is contrary to the prediction of Eq. (16) but may indicate an interaction between inlet conditions and the confinement period τ. It was found in [17,18] that low inlet compressibility broadened the range of pressure fluctuations to higher frequencies, as also illustrated in Fig. 4, [15]. Reduction in τ and consequent reduction in the initial length of liquid slugs makes the flow more homogeneous and reduces the fluctuations in the acceleration pressure drop.

It is clear that much more remains to be done to improve the modelling of pressure fluctuations. In the absence of data at high pressures, the current simple model predicts that the fluctuations are important at low pressures but decrease rapidly with increasing pressure in proportion to $[\rho_v^2 h_{lg}]^{-1}$..

Table 3

Pressure fluctuation in 1 mm tube at G =100 kg/m^{2}s, q = 100 kW/m^2, τ = 0.1 s

pressure, kPa	100	200	400	800	1400
Δp water, kPa	127	36	10	3	1
Δp R134a, kPa	17	4.8	1.4	0.38	0.13

Thome et al. [22] 3-zone heat transfer model

The Thome et al. model shares some features with the pressure fluctuation model. The period τ between confined bubbles has to be specified. The wall heat flux q to the fluid is uniform, implying that there can be no periodic storage and release of heat by the wall. The volume of the thin liquid film round a bubble is assumed negligible, so that a liquid slug has the same velocity as the adjacent bubbles. However, the liquid film does not necessarily extend over the full length of the bubble. The initial thickness is specified, either by a correlation based on local velocity or by statistical matching to a data base for time-averaged heat transfer coefficient. The film then evaporates by steady conduction at the wall heat flux q to a specified minimum thickness for stability, defining an evaporation time and a time-averaged heat transfer coefficient for the film zone. (The fate of the unevaporated liquid is not considered). After this dryout, there is single-phase transfer from the wall to the vapour. The single-phase heat transfer coefficients to the liquid slug and the vapour zone are calculated from correlations for steady, fully-developed flow. The local time averaged heat transfer coefficient is calculated from the fractional time for 2 or 3 zones. The times for the passage of liquid and vapour are calculated from the local thermodynamic quality, assuming equal phase velocities. If the bubble time exceeds the film evaporation time, dryout occurs. The fluid temperature for all the heat transfer processes is the saturation temperature for the local (steady) pressure. There

is no contribution from local nucleate boiling but it could be added in principle.

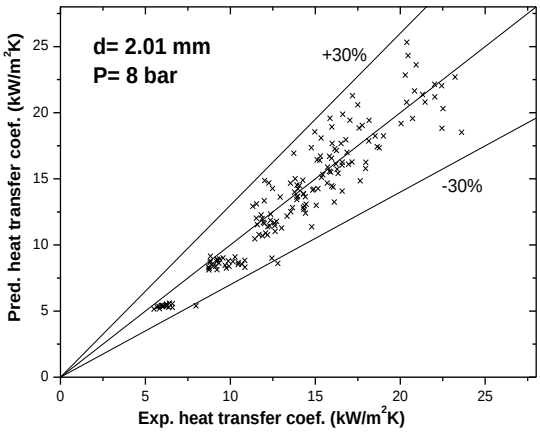

Figure 16. Comparison of the local heat transfer coefficient predicted by Thome et al [22] model and the experimental results for the D=2.01 mm tube at 8 bar.

The model was shown to correlate the data from the present study of R134a in 4.26 and 2.01 mm tubes just as well as correlations combining nucleate and convective boiling, see figure 16, [68]. Its predictions of the axial variation of heat transfer coefficient were compared with data from these tubes and the 1.1mm tube [90]. Further examples were given by Shiferaw in [37]. These indicated that the model represented reasonably well the magnitude and axial variation of the data from a low quality at which confined flow was established up to the quality at which there was a substantial rate of decline of heat transfer coefficient with quality, attributed in the earlier discussion of the R134a data to transient dryout. The model did not capture accurately the trends with changing diameter and pressure. The axial distributions were improved beyond the "transient dryout" point, at the expense of the upstream agreement, by fine-tuning the recommended values of the three crucial parameters, initial and minimum film thickness and confinement frequency / period, figure 17. This is unsurprising, since the original recommended values were based on fitting the model to a database for a wide range of fluids and pressures. It was suggested that the minimum film thickness should be the measured surface roughness, [68, 90].

The periodic dryout feature in the model means that it can predict the initial decrease in heat transfer with increasing quality, More detailed measurements of local fluctuations and analysis will be required to determine whether the modelling with optimised parameters captures the physics correctly there and also in the "transient dryout" region at higher quality before the transition to annular flow, e.g. by showing whether the fluctuations in temperature correspond to the confinement frequency. The model in its present form that excludes the effect of the wall thermal capacity cannot be expected to predict accurately high transient wall temperatures that might hinder rewetting of the wall. The 3-zone model shows promise but requires further development.

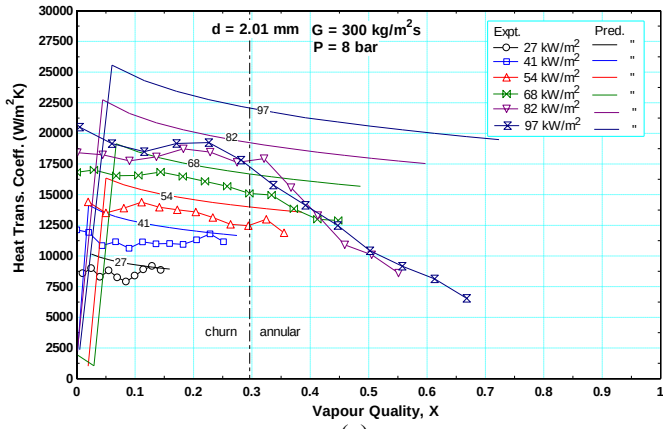

(a)

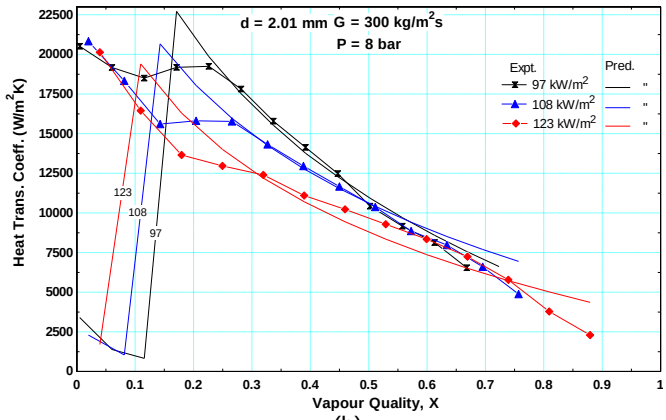

(b)

Figure 17. Comparison of Thome et al. [22] model with data for 2.01 mm tube at 8 bar , 300 kg/m^{2}s
(a) with original parameters
(b) with optimized parameters [37].

Improvements to 1-D models

The Thome et al. [22] model identifies three important influences on convective heat transfer: the bubble nucleation and early growth processes that define the period between confined bubbles, the formation of the thin liquid film and its survival. Simple modelling assumptions that make it possible to calculate the time-averaged heat transfer coefficient without having to track individual bubbles in an axial computational grid lead to some apparent physical inconsistencies. Use of the thermodynamic quality to calculate the fractional times for liquid and vapour implies inter-phase equilibrium with uniformity of temperature in the liquid and vapour at the saturation temperature. The heat supplied to the liquid slug and to the vapour in the dryout region must somehow be used to evaporate liquid and this is not taken into account in the calculation of the heat transfer coefficients. There must be perfect mixing in each phase, without bulk superheating of the liquid slug or the vapour by the uniform heat flux from the wall. Bulk superheating was measured in [15] and in the boiling of R134a in the 0.52 mm tube at very low heat fluxes [53]. Implicitly, liquid slugs survive until $x = 1$ but slug flow is observed to break down at $x \leq 0.5$.

The models of Kenning et al. [10] for a single bubble and of Faghri and associates [7,85,86] for multiple, pulsating bubbles solve the energy and momentum equations simultaneously to allow for the link between changes in pressure and bubble growth. Both require bubble tracking,

with consequent increase in computational effort. Although they employ some different physical assumptions, they have the same general issues as the Thome model [22].

The vapour phase temperature and pressure are assumed to be uniform in all three models. In [10], the temperatures of the vapour and liquid-vapour interface are assumed to be the saturation temperature for the uniform pressure in the bubble, as in [22]. In [7,85,86], the uniform temperature is calculated from an energy equation for the vapour as an ideal gas with simultaneous heat inputs and outputs where the same bubble is in contact with wall regions at different constant temperatures. The vapour temperature is not equal to the saturation temperature for the bubble pressure and a surprising feature is that the conduction through the liquid film is calculated using the difference between this temperature and the wall temperature. This raises general questions about modelling assumptions of uniformity of pressure in long bubbles, the degree of mixing by circulation in the vapour phase and the thermal resistance between the bulk vapour and the liquid-vapour interface. In [10], the bulk temperature of the liquid slug remains at the initial superheat, with some limited heat transfer to the hemispherical end of the bubble. In [7, 85, 86], the liquid slug mass and temperature are calculated by conservation equations and heat transport by the liquid is identified as the dominant mechanism. Mixing by circulation in the bulk liquid and vapour is driven by interfacial shear stresses that also influence the thickness of the liquid film. There have been many studies for steady flow of single confined bubbles and trains of bubbles at low Reynolds numbers relevant to chemical microreactors and mixers, including those reviewed in [8]. There have been few quantitative studies of the unsteady flows at high Reynolds numbers and very high accelerations relevant to flow boiling. Thome et al. [22] use a modification of a correlation derived from an experimental study of confined vapour bubble growth by Moriyama and Inoue [91], according to which the ratio of film thickness to channel diameter depends on the Capillary number *Ca* and a Bond number *Bo* in which the gravitational acceleration is replaced by the bubble acceleration. This is an interesting approach but some of the issues with its implementation are discussed in [10]. The modelling in [10] uses constant values of film thickness and length to match a small databank. [7, 85, 86] calculates a variable thickness and length by matching a hemispherical cap to the end of a polynomial approximation to the shape of a thin film moving under the influence of a finite contact angle. The hemispherical shape implicitly excludes the effect of liquid inertia at high *Re*. Further studies are required of film formation in boiling.

Only the model in [10] addresses the influence of the thermal capacity of the liquid film and the wall but the model has to be extended to handle cyclic variations, instead of the passage of a single bubble. The Thome model [22] assumes that confined bubbles form with perfect regularity at one location. The power density distributions of pressure fluctuations at low pressures in [15, 17, 18] show that the fluctuations cover a band of frequencies dependent on inlet conditions of subcooling and compressibility. The video observations in [15], discussed further in [92,93], show that there may be interaction between the pressure fluctuations and nucleation at irregular sites, complicated by delays of tens of milliseconds as visible nuclei move along the wall while coalescing or gradually growing big enough to be confined.

CONCLUSIONS

The paper presented part of the work and available results of a long term study on flow patterns, pressure drop and heat transfer rates in flow boiling in small vertical tubes (D=4.26, 2.88, 2.01, 1.10 and 0.52 mm) using R134a. The following conclusions can be stated:

1. The flow patterns in the larger tubes studied included typical structures found in macro-tubes, namely: dispersed bubbly flow, bubble flow, slug, churn, annular and mist flow. When the diameter was reduced to 2.01 the vapour slug became thinner and the liquid-vapour interface of the churn flow less chaotic. Confined flow appeared for a limited range of conditions at the lowest pressure. It became more prevalent at all pressures in the 1.1 mm tube, suggesting that a tube size of about 2 mm might distinguish fluid mechanical behaviour in macro and small tubes for R134a. Further changes were evident when the diameter was reduced to 0.52 mm, i.e. the dispersed bubble flow disappeared and the transition form slug flow to annular was through a wavy film flow. This is indicative of a possible second, maybe gradual threshold as the diameter is reduced below 1 mm.
2. Even the largest tube in the study demonstrated a departure from conventional macro-tube behaviour with respect to the development of the heat transfer coefficient as the quality increased along the tube. The heat transfer results of the 4.26 to 1.10 mm tube indicate two basic characteristics: At low qualities, the coefficient increased with increasing heat flux but was nearly independent of quality and mass flux. At higher qualities, the lines for different heat fluxes converged on a single line of heat transfer coefficient decreasing with increasing quality. Wall temperatures fluctuated in this region and the decrease was attributed to transient dryout. In macro-tubes, a region of heat transfer coefficient independent of heat flux but increasing with quality and mass flux would be expected before a sudden decrease at dryout.
3. The heat transfer and pressure drop characteristics of the 0.52 mm tube are different and are currently being re-examined. They could indicate the increasing importance of different surface characteristics as the scale diminishes. In all tubes studied, the local surface variation may affect the heat transfer characteristics.
4. A comparison of the heat transfer results with past correlations concluded that the Zhang et al. correlation [75], which is based on the traditional approach of nucleate and convective contributions predicted the current data for the 4.26 – 1.1 mm tubes prior to transient dryout fairly well when the Foster and Zuber [81] term was replaced by the Cooper correlation [82]. The Gungor and Winterton correlation [73] also predicted the data well. Neither correlation predicted the data for the 0.52 mm tube well. A method of predicting the onset of transient dryout is required.
5. The heat transfer coefficients in the 4.26 – 1.1 mm tubes at lower quality –prior to transient dryout- were consistent with the "macro tube" diagnosis of nucleate boiling but were also predicted reasonably well by the 3-zone convective boiling model of Thome et al. [22]. With adjustment to its parameters, this model could also predict the region of decreasing heat transfer coefficient at higher qualities. The 3-zone model is a suitable basis for further development discussed in the paper.

6. The pressure drop was found to increase with mass flux and decrease with pressure. It also increases with heat flux except at high heat flux values where dryout may occur. The pressure gradient increases significantly with decreasing diameter.

7. The frictional component is indeed the dominant term. However, the acceleration term is not negligible; it increases with increasing exit quality, also contributing an increasing fraction of the total pressure drop.

8. The pressure drop results were compared with existing models and correlations. The Chisholm and the Lockhart-Martinelli separated model predict the results better that the other correlations. The results of the 0.52 mm tube were not predicted well by any of the existing correlations.

NOMENCLATURE

Bo	Bond number (eq 4)
C	Constant (eq. 13)
Ca	Capillary number ($Ca=\sigma\mu/U$)
Co	Confinement number (eq 2)
D	Internal diameter, m
Eo	Eotvos number, (eq. 3)
f	Growth factor (eq. 14) sec^{-1}
F	Enhancement factor α_c/α_l (see figure 1, 2)
F	Nondimensional diameter ($F=D\rho\sigma/\mu^2$)
J^*_g	Nondimensional superficial velocity
G	mass flux, kg/m²·s
G	gravitational acceleration, m/s²
H	Enthalpy, J/kg
k	Conductivity, W/mK
L	Length, m
M	Mass flow rate, kg/s
P	Pressure, bar
Q	Heat flux, W/m^2
Q	Total Heat, W
Re	Reynolds number, ($Re = G \cdot D/\mu$)
T	Time, sec.
T	Temperature, ^0C
X	Vapour quality
X	Martinelli parameter
U	Velocity (m/s)
We	Weber number ($We= \rho U^2 D/\sigma$)
Z	Distance along the tube axis (m)

Greek Symbols

α	Heat transfer coefficient. W/m^2K
Δ	Difference
μ	Dynamic viscosity, kg/m·s
υ	Void fraction
ρ	Density, kg/m^3
τ	Period, sec.
σ	Surface tension, N/m
ϕ^2	Two-phase multiplier

Subscripts

a	acceleration component
b	bubble
c	convective
e	exit
f	friction
g	gas/vapour
i	inner
l	liquid
tp	two-phase
o	outer
sat	saturated
w	wall
z	z direction

REFERENCES

1. D.B.R. Kenning and M.G. Cooper, Saturated flow boiling of water in vertical tubes, Int. J. Heat Mass Transfer, vol. 32, pp. 445-458, 1989.
2. S.G. Kandlikar, Fundamental issues related to flow boiling in minichannels and microchannels, *Exp. Thermal and Fluid Science,* vol. 26, pp. 389-407, 2002.
3. J.R. Thome, State-of-the-art overview of boiling and two phase flows in mirochannels, Heat Transfer Engineering, vol. 27, pp. 4-19, 2006.
4. K. Cornwell and P.A. Kew, Boiling in small parallel channels, in P.A. Pilavachi (ed.), Energy Efficiency in Process Technology, pp. 624-638, Elsevier, NY, 1993.
5. A. Ullmann, N. Brauner, The prediction of flow pattern maps in minichannels, Multiphase Science and Technology, vol. 19, pp. 49-73, 2007.
6. M.K Akbar, D.A. Plummer and S.M. Ghiaasiaan, On gas liquid two-phase flow regimes in microchannels, Int. J. Multiphase Flow, vol. 29, pp. 855-865, 2003.
7. Y. Zhang and A. Faghri, Advances and unsolved issues in pulsating heat pipes, Heat Transfer Engineering, vol. 29, pp. 20-44, 2008.
8. P. Ausillous and D. Quéré, Quick deposition of a fluid on the wall of a tube, Phys. Fluids, vol. 12, pp. 2367-71, 2000.
9. A. de Ryck, The effect of weak inertia on the emptying of a tube, Phys. Fluids 14 (2002) 2102–2108, and 4100.

10. D.B.R. Kenning, D.S. Wen, K.S. Das, and S.K. Wilson, Confined growth of a vapour bubble in a capillary tube at initially uniform superheat: experiments and modelling, Int. J. Heat Mass Transfer, vol. 49, pp. 4653-4671, 2006.
11. L. Zhang, K.E. Goodson and T.W. Kenny, Silicon Microchannel Heat Sinks,Theories and Phenomena, Springer Verlag, Berlin, Heidelberg, New York, 2003.
12. L. Zhang, E.N. Wang, K.E. Goodson and T.W. Kenny, Phase change phenomena in silicon microchannels, Int. J. Heat Mass Transfer, vol. 48, pp.1572–1582, 2005.
13. S.G. Kandlikar, W.K. Kuan, D.A. Willistein and J. Borrelli, Stabilization of flow boiling in microchannels using pressure drop elements and fabricated nucleation sites, J. Heat Transfer, vol. 128, pp. 389-396, 2006.
14. A. Koşar, C. J. Kuo and Y.Peles, Boiling heat transfer in rectangular microchannels with reentrant cavities, Int. J. Heat Mass Transfer, vol.48, pp. 4867–4886, 2005.
15. D.B.R. Kenning and Y. Yan, Saturated flow boiling of water in a narrow channel: experimental investigation of local phenomena, IChemE Trans. A, Chem. Eng. Res. And Design, vol. 79, pp. 425-436, 2001.
16. D.S. Wen, D.B.R. Kenning and Y. Yan, Flow boiling of water in a narrow vertical channel at low mass flux: observations of local phenomena, Proc.12th Int.Heat Transfer Conf. Grenoble, vol. 3, pp. 773-778, 2002.
17. D. Brutin, F. Topin and L. Tadrist, Experimental study of the unsteady convective boiling in heated minichannels, Int. J. Heat Transfer, vol.46, pp. 2957-2965, 2003.
18. D. Brutin and L. Tadrist, Pressure drop and heat transfer analysis of flow boiling in a minichannel; influence of the inlet condition on two-phase flow stability, Int. J. Heat Mass Transfer, Vol.47, pp. 2365-2377, 2004.
19. A. Koşar, C. J. Kuo and Y.Peles, Suppression of boiling flow oscillations in parallel microchannels by inlet restrictions, J. Heat Transfer, vol. 128, pp. 251-260, 2006.
20. P.C. Lee and C. Pan, Boiling heat transfer and two-phase flow of water in a single shallow microchannel with a uniform or diverging cross-section, J. Micromech. Microengineering, vol. 18, 025005, 2008.
21. G.P. Celata, Single-and two-phase flow heat transfer in micropipes, 5th European Thermal Sciences Conf., Eindhoven, The Netherlands, 2008.
22. J.R. Thome, V. Dupont and A.M. Jacobi, Heat transfer model for evaporation in microchannels, Part I: Presentation of the model, Int. J. Heat Mass Transfer, vol. 47, pp. 3375-3385, 2004.
23. J.R. Thome, V. Dupont and A.M. Jacobi, Heat transfer model for evaporation in microchannels, Part II: Comparison with the data base, Int. J. Heat Mass Transfer, vol. 47, pp. 3387-33401, 2004.
24. X. Huo, L. Chen, Y.S. Tian, and T.G. Karayiannis, Flow boiling heat transfer and flow patterns in small tubes, Applied Thermal Engineering, Vol. 24, pp. 1225 – 1239, 2004.
25. L. Chen, Y.S. Tian and T.G. Karayiannis, Two-phase flow patterns in small diameter tubes, Proc. Inst. Mech. Engrs, J. Process Mechanical Engineering, Vol. 219, (Part E), pp. 167-181, 2005.
26. X. Huo, Experimental study of flow boiling heat transfer in small diameter tubes, PhD Thesis, London South Bank University, 2005.
27. X. Huo, D. Shiferaw, T.G. Karayiannis and D.B.R. Kenning, Two-Phase Pressure Drop in small to mini diameter tubes, 6th Int. Conf. on Enhanced, Compact and Ultra-compact heat exchangers, Germany, Sept. 2007.
28. J.G. Collier and J.R. Thome, Convective boiling and condensation, Oxford Science Publications, 3rd ed., 1996.
29. B. Massey and J. Ward-Smith, Mechanics of Fluids. Stanley Thornes Ltd, 7th edition, 1998.
30. F.W. Dittus, L.M.K. Boelter, Heat transfer in automobile radiators of tubular type, Univ. California, Berkeley, Publ. Eng. 2/13, pp. 443-461, 1930.
31. B.S. Petukhov, Heat transfer and friction in turbulent pipe flow with variable physical properties, Adv. in Heat Transfer, Academic Press New York, 6, pp. 503-564, 1970.
32. V. Gnielinski, New equations for heat and mass transfer in turbulent pipe and channel flow, International Chemical Eng., 16 pp. 359–368., 1976.
33. V. Gnielinski, VDI-Wärmeatlas, Springer-Verlag, Berlin, Heidelberg, 1997.
34. T.M. Adams, S.I. Abdel-khalik, S.M. Jeter and Z.H. Qureshi, An Experimental Investigation of Single-Phase Forced Convection in Micro-Channels, Int. J. Heat Mass Transfer, Vol.41, No. 6-7, pp. 851-857, 1998.
35. S.B. Choi, R.F. Barron and R.O. Warrington, Fluid flow and heat transfer in microtubes, Micromechanical Sensors, Actuators and Systems, ASME DSC, vol. 32, pp. 123–128, 1991.
36. D. Shiferaw, M.M. Mahmoud, T.G. Karayiannis and D.B.R. Kenning, Experimental flow boiling study in a 0.52 mm diameter vertical tube using R134a, 5th European Thermal-Sciences Conference, Eindhoven, 2008.
37. D. Shiferaw, Two-phase flow boiling in small – to micro – diameter tubes, PhD Thesis, Brunel University, 2008.
38. J.W. Coleman and S. Garimella, Characterization of two-phase flow patterns in small diameter round and rectangular tubes, International Journal of Heat and Mass Transfer, Vol. 42, pp. 2869-2881, 1999.
39. T. Oya, Upward liquid Flow in small tube into which air streams (1st Report, Experimental apparatus and flow patterns), Vol. 14, No. 78, pp. 1320-1329, 1971.
40. L. Chen, Y.S. Tian and T.G. Karayiannis, The effect of tube diameter on vertical two-phase flow regimes in small diameter tubes, Int. Journal Heat and Mass Transfer, Vol. 49, pp. 4220-4230, 2006.
41. D. Barnea, Y. Luninski, Y. Taitel, Flow pattern in horizontal and vertical two phase flow in small diameter pipes, The Canadian Journal of Chemical Engineering, Vol. 61, No. 5, pp. 617-620, 1983.
42. D.A. Damianides and J.W. Westwater, Two-phase flow patterns in a compact heat exchanger and in small tubes, Second UK National Conference on Heat Transfer, Vol. 11 Sessions 4A-6C, pp. 1257-1268, 1988.
43. K. Mishima, and T. Hibiki, Some characteristics of air-water two-phase flow in small diameter vertical tubes, Int. J. Multiphase flow, Vol. 22, No. 4, pp. 703-712, 1996.
44. P.A. Kew and K. Cornwell, Correlations for the prediction of boiling heat transfer in small diameter channels, Applied Thermal Eng., vol.17, pp. 705-715, 1997.
45. S. Lin, P.A. Kew and K. Cornwell, Two-phase flow regimes and heat transfer in small tubes and channels, Heat Transfer1998, Proceedings of 11th IHTC, Vol. 2, August 23-28, Kyongju, Korea, pp. 45-50, 1998.
46. K.A. Triplett, S.M. Ghiaasiaan, S.I. Abdel-Khalik and D.L. Sadowski, Gas-liquid two-phase flow in microchannels, Part I: Two-phase flow patterns, Int. J. of Multiphase Flow, Vol. 25, Elsevier Science Ltd., pp. 377-394, 1999.
47. T.S. Zhao and Q.C. Bi, Co-current air-water two-phase flow patterns in vertical triangular microchannels. Int. J. Multiphase Flow, 27, pp. 765-782, 2001.
48. A. Serizawa, Z. Feng, Z. Kawara, Two phase flow in microchannels, Exp. Thermal Fluid Sci., vol. 26, pp. 703-714, 2002.

49. A. Kawahara, P.M.-Y. Chung and M. Kawaji, Investigation of two-phase flow patterns, void fraction and pressure drop in a micro-channel, Int. J. Multiphase Flow, Vol. 28, pp. 1411–1435, 2002.
50. P. M. Y. Chung and M. Kawaji, The effect of channel diameter on adiabatic two-phase flow characteristics in microchannels, Int. J. Multiphase Flow, vol. 30, pp. 735-761, 2004.
51. R. Xiong and J.N. Chung, An experimental study of the size effect on adiabatic gas-liquid two-phase flow patterns and void fraction in microchannels, Phys. Fluids, Vol. 19, 2007.
52. R. Revellin, J.R. Thome, A new type of diabatic flow pattern map for boiling heat transfer in microchannels, J. Micromech. Microeng. 17, pp. 796, 2007.
53. T.G. Karayiannis, D. Shiferaw, D.B.R. Kenning and V.V. Wadekar, Flow patterns and heat transfer in small to micro diameter tubes, Submitted, J. Heat Transfer Eng., 2008.
54. L. Chen, Y.S. Tian, T.G. Karayiannis and D.B.R. Kenning, Flow patterns and flow regime transitions for vertical upward two-phase flow in small diameter tubes, Part I: Experimental results, In preparation.
55. L. Chen, Y.S. Tian, T.G. Karayiannis and D.B.R. Kenning, Flow patterns and flow regime transitions for vertical upward two-phase flow in small diameter tubes, Part II: Modelling study, In preparation
56. R.C. Martinelli and D.B. Nelson, Prediction of pressure drop during forced-circulation boiling of water, Trans. ASME, vol. 70, pp. 695 – 702, 1948.
57. D. Chisholm, Two-phase flow in pipelines and heat exchangers. Longman, New York, 1983.
58. T.N. Tran, M.C. Chyu, M.W. Wambsganss and D.M. France, Two phase pressure drop of refrigerants during flow boiling in small channels: an experimental investigation and correlation development, Int. J. Multiphase Flow 26, pp. 1739-1754, 2000.
59. M. Kureta, T. Kobayashi, K. Mishima and H. Nishihara, Pressure drop and Heat Transfer for flow boiling of water in small diameter tubes, JSME International Journal, Series B, Vol. 41, No. 4, 1998.
60. G. Ribatski, L. Wojtan, J.R. Thome, Analysis of experimental data and prediction methods for two-phase frictional pressure drop and flow boiling heat transfer in micro-scale channels, Experimental Thermal and Fluid Science, Vol.31, pp. 1-19, 2006.
61. D.S. Wen and D.B.R. Kenning, Two-phase pressure drop of water during flow boiling in a vertical narrow channel, Experimental Thermal and Fluid Science, Vol. 28, pp. 131-138, 2004.
62. W. Yu, D.M. France, M.W. Wambsganss and J.R. Hull, Two phase pressure drop, boiling heat transfer, and critical heat flux to water in small-diameter horizontal tube, Int. J. Multiphase Flow, Vol. 28, pp. 927-941, 2002.
63. R.G. Warrier, K.V. Dhir and A.L. Momoda, Heat transfer and pressure drop in narrow triangular channels, Exp. Thermal and Fluid Sc., Vol. 26, pp. 53-64, 2002.
64. H. J. Lee and S. Y. Lee, Pressure drop correlation for two-phase flow within horizontal rectangular channels with small height, Int. J. of Multiphase Flow, Vol. 27, pp. 783-796, 2001.
65. W. Qu and I. Mudawar, Measurement and prediction of pressure drop in two-phase micro-channel heat sinks, Int. Journal of Heat Mass transfer, Vol. 46, pp. 2737 – 2753, 2003.
66. D. Chisholm, Two-phase flow in pipelines and heat exchangers. Longman, New York, 1983.
67. H. Muller-Steinhagen, K., Heck, A simple friction pressure drop correlation for two-phase flow in pipes, Chem. Eng. Proc., Vol. 20, pp. 297–308, 1986.
68. D. Shiferaw, X. Huo, T.G. Karayiannis and D.B.R Kenning, Examination of heat transfer correlations and a model for flow boiling of R134a in small diameter tubes, Int. J Heat Mass Transfer, Vol. 50, pp. 5177-5193, 2007,.
69. W.M. Rohsenhow, A method of correlating heat transfer data for surface boiling of liquids, ASME Trans. J. applied Mechanics, 74, pp. 969-976, 1952.
70. S.S. Kutateladze, Boiling heat transfer, Int. J. Heat Mass Transfer, Vol. 4, pp. 31-35, 1961 .
71. M. M. Shah, a new correlation for heat transfer during flow boiling through pipes, ASHRAE Tans. 82 (2), pp. 66-86, 1976.
72. J.C. Chen, A correlation for boiling heat transfer to saturated fluid in convective flow, Ind. Eng. Chem. Process Des. Dev. Vol. 5, No 3, pp. 322-329, 1966.
73. K.E. Gungor and R.H.S. Winterton, A general correlation for flow boiling in tubes and annuli. Int. J.Heat Mass Transfer, 29, pp. 351-358, 1986.
74. Z. Liu and R.H.S. Winterton, A general correlation for saturated and subcooled flow boiling in tubes and annuli, based on a nucleate pool boiling equation. International Journal Heat Mass Transfer, 34(11), pp. 2759-2766, 1991.
75. W. Zhang, T. Hibiki, and K. Mishima, Correlation for flow boiling heat transfer in mini-channels. Int. J. Heat Mass Transfer, 47, pp. 5749-5763, 2004.
76. S. Saitoh, H. Daiguji, and E. Hihara, Correlation for boiling heat transfer of R134a in horizontal tubes including effect of tube diameter. Int. J. Heat Mass Transfer, 50, pp. 5215-5225, 2007.
77. G.M. Lazarek and S.H. Black, Evaporative heat transfer, pressure drop and critical heat flux in a small vertical tube with R-113. Int. J. Heat Mass Transfer, 25(7), pp. 945-960, 1982.
78. T.N. Tran, M.W. Wambsganss and D.M. France, Small circular- and rectangular-channel boiling with two refrigerants. Int. J. Multiphase Flow, 22(3), pp. 485-498, 1996.
79. S.G. Kandlikar and P. Balasubramanian, An extension of the flow boiling correlation to transition, laminar, and deep laminar flows in minichannels and microchannels, Heat Transfer Eng., 25(3), pp. 86-93, 2004.
80. S. G. Kandlikar, A general correlation for saturated two-phase flow boiling heat transfer inside horizontal and vertical tubes, J. Heat Transfer, 112, pp. 219-228, 1990.
81. H.K. Foster and N. Zuber, Dynamics of vapour bubbles and boiling heat transfer, AIChe J. 1, pp. 531-535, 1955.
82. M.G. Cooper, Saturated nucleate pool boiling – a simple correlation. In first UK National Heat Transfer Conf., IChemE Symposium, Series 86, 2, pp. 785-793, 1984.
83. P.A. Kew and K. Cornwell, On pressure fluctuations During boiling in narrow channels, Proc. 2nd European Thermal Sciences and 14th UIT National Heat Transfer Conf.,Rome, Vol. 3, pp. 1323-1327, 1996.
84. A.M. Jacobi and J.R. Thome, Heat transfer model for evaporation of elongated bubble flows in microchannels, J. Heat Transfer, vol. 124, pp. 1131-1136, 2002.
85. M.B. Shafii, A. Faghri and Y. Zhang, Thermal modelling of unlooped and looped pulsating heat pipes, J. Heat Transfer, Vol. 123, pp. 1159-1172, 2001.
86. M.B. Shafii, A. Faghri and Y. Zhang, Analysis of heat transfer in unlooped and looped pulsating heat pipes, Int. J. Numerical Methods for Heat and Fluid Flow, Vol. 12, pp. 585-609, 2002.
87. W. Qu and I. Mudawar, Flow boiling heat transfer in two-phase microchannel heat sinks – II. Annular two-phase

flow model, Int. J. Heat Mass Transfer, Vol. 46, pp. 2773-2784, 2003.
88. H. Boye, Y. Staate and J. Schmidt, Experimental investigation and modelling of heat transfer during convective boiling in a minichannel, Int. J. Heat Mass Transfer, vol. 50, pp. 208-215, 2007.
89. Y.P. Peles, L.P. Yarin and G. Hetsroni, Steady and unsteady flow in a heated capillary, Int. J. Multiphase Flow, vol. 27, pp. 577-598, 2001.
90. D. Shiferaw, T.G. Karayiannis and D.B.R Kenning, Flow boiling in a 1.1 mm tube with R134a: Experimental results and comparison with a model, Int. J. Thermal Sciences, doi:10.1016/j.ijthermalsci.2008.02.009, 2008.
91. K. Moriyama, A. Inoue, Thickness of the liquid film formed by a growing bubble in a narrow gap between two horizontal plates, J. Heat Transfer, vol.118, pp.1223–1230, 1996.
92. D.S.Wen, K.S Das, S.K. Wilson and D.B.R. Kenning, Initiation and growth of confined vapour bubbles in micro-channels, 9th UK Nat. Heat Transfer Conf., 2005.
93. D.S. Wen, Flow boiling heat transfer in micro-geometries, D.Phil. Thesis, University of Oxford, 2004.

Appendix A

Table A1. Mean average error (MAE) and percentage of data within ±30% (β) for pressure correlations.

Models and Correlations	Tube Internal diameter (mm)					
		4.26	2.88	2.01	1.10	0.52
Homogeneous Model	MAE (%) β (%)	24.5 75	19.8 83	20.5 70	27 65	62 0
Separated Model	MAE (%) β (%)	14 90	23.4 81	21 82	25 75	56 12
Chisholm [66]	MAE (%) β (%)	15.1 91	23.5 80	16.3 88	27 74	35 40
Tran et al. [58]	MAE (%) β (%)	197 0	285 0	221 0	260 0	152 16.5
Mishimal and Hibiki [43]	MAE (%) β (%)	16 92	19.7 82	19.7 70	35.6 40	75 0
Muller-Steinhagen and Heck [67]	MAE (%) β (%)	45 5	77 28	62 16	59 23	88 0

Table A2. Mean average error (MAE) and percentage of data within ±30% (β) for heat transfer correlations.

Models and correlations	Tube internal diameter (mm)					
		4.26	2.88	2.01	1.10	0.52
Lazarek and Black [77]	MAE (%) β (%)	33.8 40	21.8 75	37 23	32.7 35	52.5 37
Tran et al. [78]	MAE (%) β (%)	15 100	16.3 97	41.3 2	52.5 0	73.1 1.5
Gungor and Winterton[73]	MAE (%) β (%)	15.3 88	8.5 100	13.2 99	12.2 99	51.2 62.5
Liu and Winterton [74]	MAE (%) β (%)	26.3 79.5	17 96	34.5 25.1	34.5 30	57 40.5
Kandlikar and Balasubramanian [79]	MAE (%) β (%)	21.1 79.5	23 73.5	20.4 80.5	48.7 25	67 5
Zhang et al. [75][1]	MAE (%) β (%)	60.5 0	53.5 1	67 0	72.5 0	144 1
Zhang et al. [75][2]	MAE (%) β (%)	7 100	10.5 99	15.1 94	19.6 86.5	50 56
Saitoh et al. [76]	MAE (%) β (%)	48.6 0	33 35	41.4 3	37.2 20	57.3 30

[1] Using Foster and Zuber [81] correlation for the nucleate boiling term as given in Zhang et al. [75].

[2] Modified Zhang et al. [75] correlation using Cooper [82] for the nucleate boiling contribution.